Astron. Astrophys. 298, 87–106 (1995)

ASTRONOMY AND ASTROPHYSICS

Age distribution of LMC clusters from their integrated UBV colors: history of star formation

L. Girardi[1,2], **C. Chiosi**[1], **G. Bertelli**[1,3], **and A. Bressan**[4]

[1] Department of Astronomy, University of Padova, Vicolo dell'Osservatorio 5, I-35122 Padova, Italy
[2] Instituto de Física, UFRGS, Caixa Postal 15051, 91501-970 Porto Alegre RS, Brazil
[3] National Council of Research (GNA), Roma, Italy
[4] Astronomical Observatory, Vicolo dell'Osservatorio 5, I-35122 Padova, Italy

Received 27 June 1994 / Accepted 20 October 1994

Abstract. In this paper we revise the relationship between ages and metallicities of LMC star clusters and their integrated UBV colors. The study stands on the catalog of UBV colors of the Large Magellanic Cloud (LMC) clusters by Bica et al. (1994; BCDSP) and the photometric models of single stellar populations (SSP) calculated by Bertelli et al. (1994).

These photometric models nicely describe the color distribution of LMC clusters in the $(U-B)$ vs. $(B-V)$ plane together with the observed dispersion of the colors and the existence of a gap in a certain region of this diagram. In the case of blue clusters, most of the dispersion in the colors can be accounted for by the presence of stochastic effects on the mass distribution of stars, whereas for the red ones additional dispersion's of ~ 0.2 dex in metallicity and of ~ 0.05 mag in color excess are needed. From comparing the observed distribution of integrated colors in the $(U-B)$ vs. $(B-V)$ diagram with the theoretical models, it turns out that: 1) The data are consistent with the presence of a gap (period of quiescence) in the history of cluster formation. If the age-metallicity relation (AMR) for the LMC obeys the simple model of chemical evolution, the gap is well evident and corresponds to the age interval ~ 3 Gyr to $(12-15)$ Gyr. On the contrary, if the chemical enrichment has been much slower than in the simple model, so that intermediate age clusters are less metal rich, the gap is expected to occur over a much narrower color range and to be hidden by effects of color dispersion. 2) The bimodal distribution of $B-V$ colors can be reproduced by a sequence of clusters almost evenly distributed in the logarithm of the age, whose metallicity is governed by a normal AMR. No need is found of the so-called phase transitions in the integrated colors of a cluster taking place at suitable ages (Renzini & Buzzoni 1986). 3) The gap noticed by BCDSP in the $(U-B)$ vs. $(B-V)$ plane can be explained by the particular direction along which cluster colors are dispersed in that part of the $(U-B)$ vs. $(B-V)$ diagram. Also in this case, no sudden changes in the integrated properties of clusters must be invoked.

The results of this analysis are used to revise the empirical method proposed by Elson & Fall (1985, EF85) to attribute ages to LMC clusters according to their integrated UBV colors. We show that the EF85 method does not provide the correct relation between ages and colors for clusters of low metallicity and hence its inability to date the old clusters. We propose two modifications to the definition of the parameter S of EF85 such that the age sequence of red clusters is suitably described, and the intrinsic errors on ages caused by the heavy presence of various effects dispersing the colors are reduced to a minimum. The age sequence is calibrated on 24 template clusters for which ages were independently derived from recent color-magnitude diagrams (CMD).

Finally, we attribute ages to all clusters present in BCDSP catalog, and derive the global age distribution function (ADF) for LMC clusters. The ADF presents new features that were not clear in previous analyses of UBV data, but were already suggested by a number of independent observational studies. The features in question are periods of enhanced cluster formation at ~ 100 Myr and $1-2$ Gyr, and a gap in the cluster formation history between ~ 3 and $(12-15)$ Gyr. The peaks observed in the distribution of $B-V$ colors are found to be sensitive to the presence of these periods of enhanced cluster formation and the lack of extremely red clusters caused by the age gap between intermediate-age and old clusters.

Key words: galaxies: Magellanic Clouds – galaxies: star clusters – stars: evolution – stars: HR diagram – Galaxy: globular clusters: general

1. Introduction

The use of the Magellanic Clouds star clusters as templates for studies of stellar populations in other galaxies, as well as indispensable tools for the calibration of stellar evolution models,

Send offprint requests to: L. Girardi

has been stressed and explored by many authors (e.g. Renzini & Buzzoni 1986; Bica & Alloin 1986; Chiosi et al. 1992 and references therein). What makes these clusters so important and different from their Galactic analogs, is the range of metallicities spanned by the youngest ones, and in general their richness. In addition to this, due to our external view of the Clouds, complete samples of clusters can be easily studied.

Until recently, data for large samples of clusters existed only in integrated photometry. Searle et al. (1980, hereafter SWB) showed that the LMC clusters can be arranged in a single sequence in the $Q(ugr) - Q(vgr)$ diagram, probably one of varying age and metallicity. Later Frenk & Fall (1982) showed that the same sequence is present in the $(U - B)$ vs. $(B - V)$ diagram, giving origin to what is known as the "equivalent" SWB sequence (E-SWB).

Many efforts have been made to rank the integrated UBV colors of the clusters as a function of their ages and metallicities as well as to derive their ADF (e.g. EF85; and Chiosi et al. 1988, hereafter CBB88). All these studies were based on the van den Bergh (1981) catalog of integrated UBV colors, which itself is an amalgam of observations from several authors. Particular care was taken in obtaining a reliable age calibration by means of cluster CMDs (eg. Elson & Fall 1988; Chiosi et al. 1985; CBB88).

Since those early studies, a lot of new observational material became available, in particular new CMDs from CCD data, and a large and homogeneous set of photometric data in integrated UBV colors (Bica et al. 1991; 1994, hereafter BCDSP). Unfortunately, with respect to the metallicities of the LMC clusters, the situation has not changed too much: different studies present significantly different results for the same clusters. So far, there is only one recent attempt to provide homogeneous metallicities for a large number of LMC clusters, namely the study of Olszewski et al. (1991).

The BCDSP data greatly improve upon the previous catalog of van den Bergh (1981). In particular, the number of clusters with integrated UBV photometry is multiplied by four, and the observational procedure (choice of apertures and comparison fields) is uniform for most of the clusters. Girardi & Bica (1993, hereafter GB93) made a preliminary analysis of BCDSP data based on a comparison with models of photometric evolution of SSPs limited to the case of solar metallicity. This study stressed the importance of stochastic effects on the distribution of UBV colors, and of the IMF slope on the derivation of the ADF (see also CBB88).

In this work, with the aid of new photometric models for SSPs we revise the relationship between ages, metallicities, and integrated UBV colors of LMC clusters. In particular, we seek for as much homogeneity as possible among the various sources of observational data and theoretical models. With respect to previous studies on this subject (e.g. EF85, CBB88, GB93), the points of major novelty are:

1) We use the new libraries of stellar tracks and isochrones of the Padova group (Bertelli et al. 1994) to calculate the integrated UBV colors of SSPs. These isochrones incorporate a number of improvements with respect to previous ones. The photometric models and their general characteristics are described in Sect. 2, together with a preliminary comparison with BCDSP data.

2) Throughout this paper, we use the BCDSP catalog as the database of integrated UBV colors of LMC clusters to be compared with the predictions of photometric models.

3) We carefully examine the effects of the underlying AMR (Sect. 3) and of different causes of dispersion in the integrated UBV colors, namely stochastic effects in the mass distribution of stars, variations in reddening and metallicities among clusters (Sect. 4). Taking them into account in models of SSPs allows us to cast light on the physical nature and characteristics of two different gaps: the gap in the distribution of $B - V$ colors reported by van den Bergh (1981), and the gap in the $(U - B)$ vs. $(B - V)$ diagram at the E-SWB group IV reported by Bica et al. (1991). These are firstly presented in Sect. 5, and later more deeply discussed at the end of Sect. 8.

4) We revise the overall method for determining the ages of LMC clusters from their integrated colors. Firstly, we choose a set of clusters with recent CCD-CMDs in order to provide robust age calibrators (Sect. 6). Secondly, we revise the EF85 method for attributing ages to individual clusters according to their integrated UBV colors. Two modifications are proposed, aimed to more properly follow the relationship between integrated UBV colors and ages. The new method is presented in Sect. 7.

Finally, in Sect. 8 we derive the ADF for LMC clusters. This clearly differs from previous ones both in quality and chief characteristics. In fact, superposed to a general decrease with age that can be interpreted as the result of dynamical disruption of the clusters, the ADF clearly shows two episodes of enhanced cluster formation rate and a major gap in the cluster formation history.

Section 9 draws a few general comments.

2. Theoretical integrated colors of star clusters

In this section we present in some detail the time evolution of the integrated magnitudes and colors of SSPs closely mimicking the star clusters.

2.1. Photometric evolution of SSPs

The evolutionary stellar models used in this study are from Bressan et al. (1993) and Fagotto et al. (1994a, 1994b), whereas the corresponding isochrones are from Bertelli et al. (1994). We refer to these works for all details.

The procedure to obtain colors of SSPs from theoretical isochrones is straightforward and will not be described in detail here (see e.g. Alongi & Chiosi 1989; GB93). Suffice it to say that the SSP models presented here (if not stated otherwise) are constructed assuming the Salpeter IMF, $\phi_m \propto m^{-(x+1)}$, with $x = 1.35$.

Figure 1 presents the time evolution of the integrated UBV colors for SSPs with different metallicities ($[Z = 0.0004, Y = 0.23]$, $[Z = 0.001, Y = 0.23]$, $[Z = 0.004, Y = 0.24]$, $[Z = 0.008, Y = 0.25]$, $[Z = 0.02, Y = 0.28]$), whereas Fig. 2

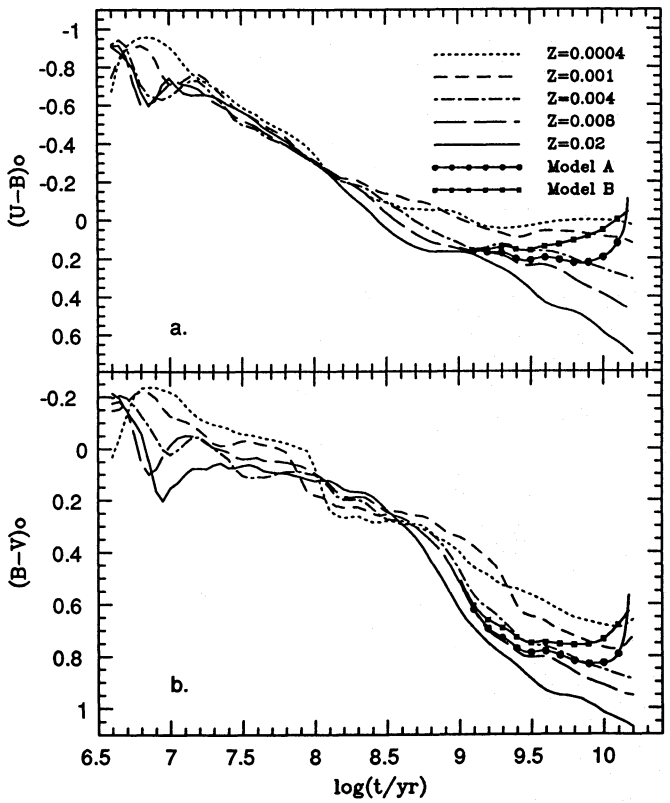

Fig. 1a and b. Time evolution of $(U-B)_0$ (panel **a**) and $(B-V)_0$ (panel **b**) colors for SSPs of different metallicities. We also plot the color-age relations of Models A and B for galactic chemical enrichment to be described later [see Eqs. (1) and (2)]. For the sake of clarity, both models are plotted just for $\log t > 9$; for younger ages they are essentially identical to the SSP with $Z = 0.008$. These models are indicated by heavy solid lines, along which time steps of $\Delta \log t = 0.1$ are marked by full dots and squares

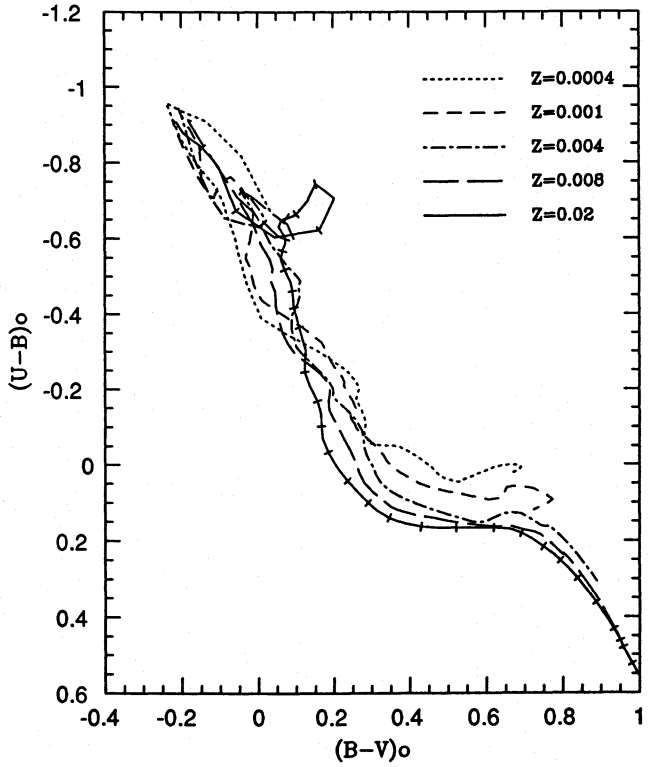

Fig. 2. The evolution in the $(U-B)$ vs. $(B-V)$ diagram of SSPs with different metallicities. All the symbols have the same meaning as in Fig. 1. The ticks along the path of the Z=0.02 SSP denote age intervals spaced by $\Delta \log t = 0.1$

shows the same in the color-color diagram. The original curves are smoothed over time steps 0.1 wide in $\log t$ in order to eliminate some sharp fluctuations, about 0.05 mag in size, along the evolutionary lines. These fluctuations are simply due to the limited number of stellar tracks used to generate the isochrones. We warn the reader that none of the results reported in this paper is affected by this smoothing.

Looking at the $Z = 0.02$ track in Fig. 1 as an example, we notice the same general behaviour already described by GB93. In particular:

1) The loop toward red $B-V$ and $U-B$ colors (Fig. 1) at the age of about 10 Myr is caused by the appearance in the SSP of the red supergiant stars (RSG). At earlier ages, the SSP has in practice no RSG stars. After that, the SSP contains a balanced population of both red and blue supergiants (for details, see GB93). This corresponds to the loop-like feature visible in Fig. 2 at $(B-V)_0 = 0.1$ and $(U-B)_0 = -0.7$.

2) The second excursion to the red at the age of 100 Myr found by GB93 does not occur. The reason for the lack of this feature resides in the different ratio between the He and H-burning lifetimes for intermediate-mass stars. This was $t_{\rm He}/t_{\rm H} \sim 0.25$ with the stellar models used by GB93 (Maeder & Meynet 1989), whereas with the present models it amounts to about 0.1. As a consequence of this, at the age interval in question (around 100 Myr) the present models of color evolution agree better with the distribution of integrated UBV colors of LMC clusters than those presented by GB93 (see Fig. 4 and compare with Fig. 3 in GB93).

Two other important characteristics of the SSP with $Z = 0.02$ are: a) The evolution in the $(U-B)$ vs. $(B-V)$ diagram proceeds at an almost constant rate of change in color by $\log t$ interval, as shown by the ticks spaced by $\Delta \log t = 0.1$ in Fig. 2. b) Two major changes of slope in the $(U-B)$ vs. $(B-V)$ plane (Fig. 2) at $(B-V)_0 \simeq 0.3$ and $(B-V)_0 \simeq 0.7$ that roughly correspond to the ages of $\log t \simeq 8.7$ and $\log t \simeq 9.2$, respectively (see Fig. 1).

Both points bear very much on problems to be discussed in this paper. In particular, point (1) sets the fundamentals of the relation between the parameter S and age first introduced by EF85 (see Sect. 7), while (2) is important with respect to the bimodality in the $B-V$ color distribution of LMC clusters (Sect. 5.3). We emphasize that, although the present models include all the relevant stellar evolutionary phases, this behaviour is mainly determined by the color evolution of the stars in the upper main sequence (MS) and in the stage of core He-burning (CHeB) (see e.g. GB93).

How does the evolutionary path of a SSP change going to lower metallicities?

For young SSPs (clusters), the RSG phase becomes progressively less pronounced, and an increasingly large jump in the $(B-V)_0$ color occurs at the age of $\sim$ 100 Myr (Fig. 1) due to the first appearance of AGB stars (see Bertelli et al. 1994; Bressan et al. 1994). Both features are not relevant to the discussion of the colors of LMC clusters. Firstly, because they do not give rise to large changes in the two-color plane, and secondly, because all the young clusters are found to possess metallicities higher than [Fe/H] = -0.7 (see Olszewski et al. 1991). However, it is worth noticing that the general behaviour of the SSPs with $Z = 0.004$ and $Z = 0.001$ correspond to the trend observed in the colors of the SMC clusters. This is shown by Fig. 1 of EF85, where SMC clusters with $U-B \lesssim -0.4$ have $B-V$ colors $\sim$ 0.15 mag bluer than LMC clusters, whereas young SMC clusters in the range $-0.4 < U-B < 0.1$ have $B-V$ colors equal-to or $\sim$ 0.1 mag redder than LMC clusters.

On the contrary, the most conspicuous and important changes in the colors of SSPs with low metallicity occur for old ages (red clusters). Figure 3 details the red part of the $(U-B)$ vs. $(B-V)$ diagram, showing how the locus of the oldest SSPs (about $\sim$ 15 Gyr) runs progressively to bluer $B-V$ and $U-B$ colors with decreasing metallicity.

3. Simple chemical models for the LMC

Considering that clusters in the LMC do not possess the same metallicity and that old clusters are likely more metal-poor than the young ones as expected from any reasonable law of metal enrichment, the above behaviour of the SSP with different metallicity gives rise to a hook in the red part of the $(U-B)$ vs. $(B-V)$ plane.

In order to illustrate better this point, we plot in Fig. 3 the locus drawn in the $(U-B)$ vs. $(B-V)$ plane by SSPs whose metallicity varies with the age (old SSPs being less metal-rich than young SSPs).

Two simple AMRs are considered: in the first the metal content Z, in the second the metallicity [Fe/H] = $\log(Z/0.02)$ decrease linearly as we go back in time, or equivalently as the age of the SSPs gets older. The AMRs are expressed by

$$\textbf{Model A:}\quad Z = 0.008\,(1 - t/15\times10^9\ \mathrm{yr}) \tag{1}$$

$$\textbf{Model B:}\quad [\mathrm{Fe/H}] = -0.4 - 1.6\,(t/15\times10^9\ \mathrm{yr}) \tag{2}$$

where t is the SSP age in years (and *not* the galactic age).

Models A and B will be used for a series of considerations throughout this paper. They correspond to two simple schemes for the chemical evolution of the LMC. The linear enrichment law of Model A [Eq. (1)] corresponds to the simple model of chemical evolution (Searle & Sargent 1972) for a galaxy with a final metal content $Z = 0.008$ at the galactic age of 15 Gyr. The alternative Model B mimics a slower metal enrichment during the early epochs of galactic evolution.

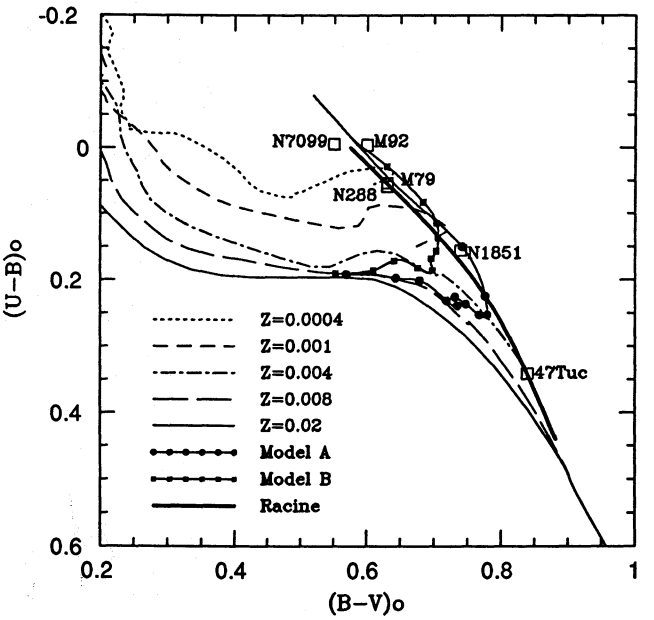

Fig. 3. Same as in Fig. 2, but detailing the region of red clusters. Models A and B are plotted only for $\log t > 9.1$; for younger ages they are similar to the SSP with $Z = 0.008$. A shift in the zero-point of $\Delta(B-V) = -0.05$ and $\Delta(U-B) = +0.03$ is applied to all the models of Fig. 2 in order to reproduce the sequence of colors for Galactic globular clusters from Racine (1976; see text). The position of a few Galactic globular clusters with known integrated colors and metallicities is also shown (open squares). The metallicities are [Fe/H] = -0.71 for 47 Tuc, -1.40 for NGC 288, -1.29 for NGC 1851, -1.69 for M 79, -2.24 for M 92, and -2.13 for NGC 7099 (Djorgovski & Meylan 1993)

We would like to call the attention on the fact that both models satisfactorily agree with the present-day observational AMRs for LMC clusters (e.g. Fig. 11 in Olszewski et al. 1991). In fact, the lack of clusters in the age interval 3 – 12 Gyr (see Sect. 5.2) does not allow us to contrive the AMR in this age range. Such an uncertainty did not occur with the old data used by Cohen (1982) and Smith et al. (1988), because of the poor estimates of cluster ages.

Plotting the evolutionary paths of the SSP in Fig. 3 a little correction to their colors has been applied. Specifically, they have been shifted by $\Delta(B-V) = -0.05$ and $\Delta(U-B) = +0.03$ in order to make the colors of the SSP with $Z = 0.004$ and $\log t = 10.2$ agree with those of 47 Tuc [$(B-V)_0 = 0.84$, $(U-B)_0 = 0.34$, and [Fe/H] = -0.71, according to the data of Djorgovski & Meylan (1993)]. With such a shift a perfect agreement between the colors of the oldest SSPs and the observational colors (solid thick line in Fig. 3) of the Galactic globular clusters given by Racine (1976) is achieved all over a wide range of metallicities. This is demonstrated by plotting on Fig. 3 the position of a few Galactic globular clusters (open squares) with metallicity going from [Fe/H] = -0.7 (47 Tuc) to [Fe/H] = -2.2 (M 92).

The reason of this marginal discrepancy between theoretical and observed colors for old clusters is not easy to understand.

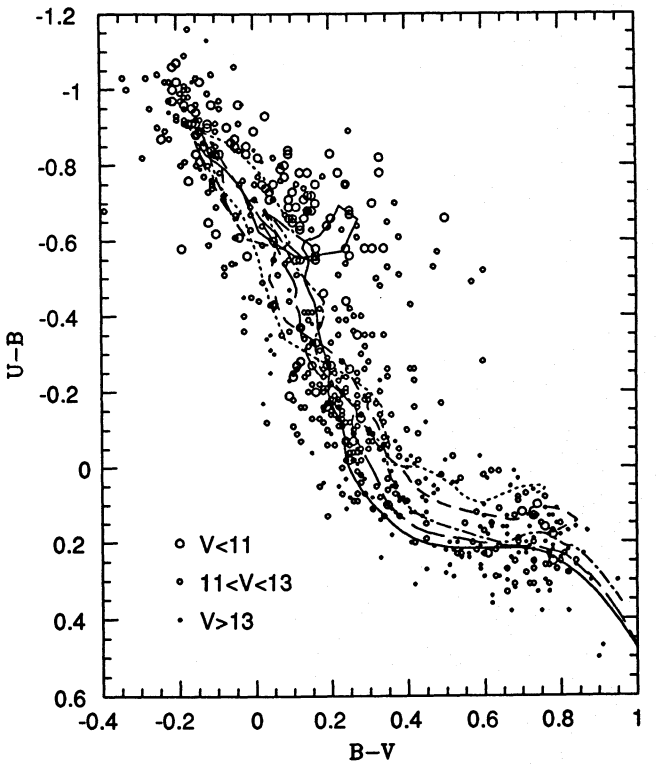

Fig. 4. Observed color-color diagram for BCDSP data (open circles). The evolutionary lines presented in Fig. 2 are superimposed, reddened by the foreground color excess $E(B-V) = 0.07$. The circles are sized according to the integrated V magnitude of the corresponding cluster

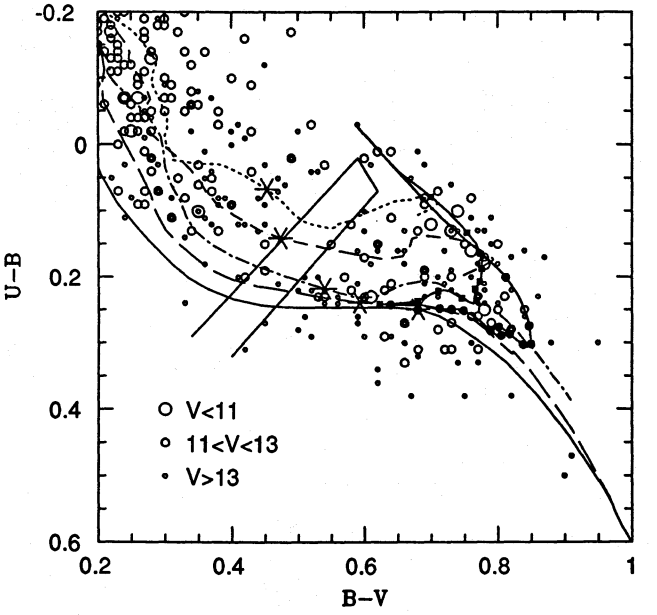

Fig. 5. The same as Fig. 4, but detailing the region of red clusters. The shift in zero-point we have discussed in the text is applied to all theoretical colors. In addition to this, we mark with big asterisks along each sequence the stage at which the RGB stars appear for the first time (approximately $\log t = 9.05$) in the SSP. The strip illustrates the gap in the distribution of clusters defined by Bica et al. (1991). Finally, Models A and B are displayed

We tentatively explored various modifications to the theory of SSPs in order to reproduce the Racine relation without shifting the colors. We tried an increase in the Reimers (1975) mass-loss parameter, η, along the RGB and AGB stages from the canonical value of 0.35 up to 1.0, and a decrease in the slope of the IMF. Changing η from 0.35 to 1.0 varies the colors by at most 0.03 mag and only in case of the low metallicity clusters ($Z \simeq 0.0004$), whereas changing the IMF slope up to $x = 0$ produces a variation $\simeq 0.02$ mag. Therefore, both are unable to shift the theoretical colors by as much as 0.05 mag in equally effective fashion for different metallicities. We conclude that the shift in the zero point probably mirrors some residual inadequacy either in the transformation from effective temperatures and luminosities to magnitudes and colors (which stands on the new grids of model atmospheres of Kurucz 1992) or in the calibration of the mixing length on the Sun (see Bertelli et al. 1994 for details). Throughout this paper we apply the correction only when comparing old SSPs with the observational data.

Figure 4 shows the color evolution of SSPs with different metallicities superimposed to the data from BCDSP. It can be seen that the SSPs agree with the general distribution of points, in particular for the brightest clusters. It is also clear that the old clusters must have metallicities lower than $Z = 0.004$, otherwise they would be much redder than observed. The reasons for the scatter in the observational data will be discussed in Sect. 4.

Figure 5 details the observed $(U-B)$ vs. $(B-V)$ diagram for the red clusters. It can be seen that Models A and B reproduce the hook of the red clusters (with SWB types V, VI and VII). However, while Model B runs through the mean locus of the data, Model A extends more to the red than the bulk of clusters. This point will be extensively commented in Sect. 5.2.

4. Possible causes of color dispersion

4.1. Stochastic effects

Previous evaluations of the amount of dispersion caused by stochastic effects in the IMF of real clusters are by CBB88 and more recently GB93 who called attention on a few important aspects of this problem. Firstly, stochastic effects could produce large dispersion's in the integrated colors of very young clusters, especially those in the RSG phase of their evolution. Secondly, the amount of dispersion varies widely along the age sequence. Thirdly, the dispersion runs along a direction that is roughly similar to that of reddening. It became also clear that in a sample with such low-luminosity clusters as that of BCDSP the inclusion of these effects is important for the interpretation of integrated colors (GB93).

To cast light on this topic, we calculate the amount of color dispersion in ensembles of clusters of same age and metallicity, and fixed integrated magnitude M_V. The procedure is similar to that adopted by CBB88 and GB93: a single theoretical cluster is generated by simulating a random distribution of stars along an

isochrone. The probability of occurrence of a given stellar mass is given by the IMF ϕ_m. Stars are added up to the cluster till its integrated magnitude reaches a certain value M_V. This allows us to compare the theoretical color distributions with that of magnitude-limited samples of data. We assume $M_V = -6$ for the integrated absolute magnitude, which approximately corresponds to the limit magnitude $V = 13$ of the BCDSP sample.

For each assigned value of age and metallicity, we perform 50 simulations of clusters. Then we estimate the mean colors $\langle B-V\rangle$ and $\langle U-B\rangle$, and the average deviations around the mean $\sigma(B-V) = \langle|B-V-\langle B-V\rangle|\rangle$ and $\sigma(U-B) = \langle|U-B-\langle U-B\rangle|\rangle$.

The results for the SSP with $Z = 0.008$ are shown in Fig. 6 which displays $\sigma(U-B)$ (top panel) and $\sigma(B-V)$ (central panel) as a function of the age. We also present the mean slope at which the dispersion occurs in the $(U-B)$ vs. $(B-V)$ plane, defined as $\alpha = \Delta(U-B)/\Delta(B-V)$ (bottom panel). The slope and associated error bars are derived from the linear least-squares fit to the color distribution at each age.

The effects of stochastic fluctuations in the star mass distribution on the integrated colors of a SSP can be summarized as follows:

- For $\log t < 6.8$ the dispersion is low, and occurs almost uniquely in the $U-B$ direction. This mirrors the lack of evolved red stars. Indeed, what changes from cluster to cluster is the distribution of stars in the upper MS, with little effect on the $B-V$ colors.
- For $6.8 < \log t \lesssim 7.4$ the dispersion is high, and does not occur along a well-defined direction. This behaviour is due to the appearance of a small number of RSG stars, whose colors are very different from those of the bright MS stars. Therefore, large differences in integrated colors arise from cluster to cluster depending on the number and magnitude of RSG stars.
- For $\log t \gtrsim 7.4$ the amount of dispersion decreases dramatically with age, due to the increasing population of post-MS stars, and the gradual decrease in the color difference between the MS-termination (TAMS) and red giant stars. The dispersion sets to a well-defined direction after $\log t \sim 8.2$, with a mean slope $\Delta(U-B)/\Delta(B-V) = 0.45$.
- For $\log t > 9.1$, with the appearance of the RGB stars, the dispersion gets very low and slightly decreasing with age, while the mean slope of the dispersion gradually increases up to $\Delta(U-B)/\Delta(B-V) \sim 0.9$. This is due to the increase in the luminosity difference between the RGB-tip and TAMS stars.

To a good approximation we can express the amount of color dispersion as a function of M_V by means of the relation

$$\sigma(B-V)_{[M_V]} \simeq \sigma(B-V)_{[M_V=-6]} \times 0.7^{(M_V+6)}. \quad (3)$$

The range of applicability is $-5 > M_V > -9$. This relation also applies to the $U-B$ color.

Repeating the analysis for lower metallicities, we get similar results, the only significant difference being that for young SSPs the dispersion is smaller because the RSG stars do not develop.

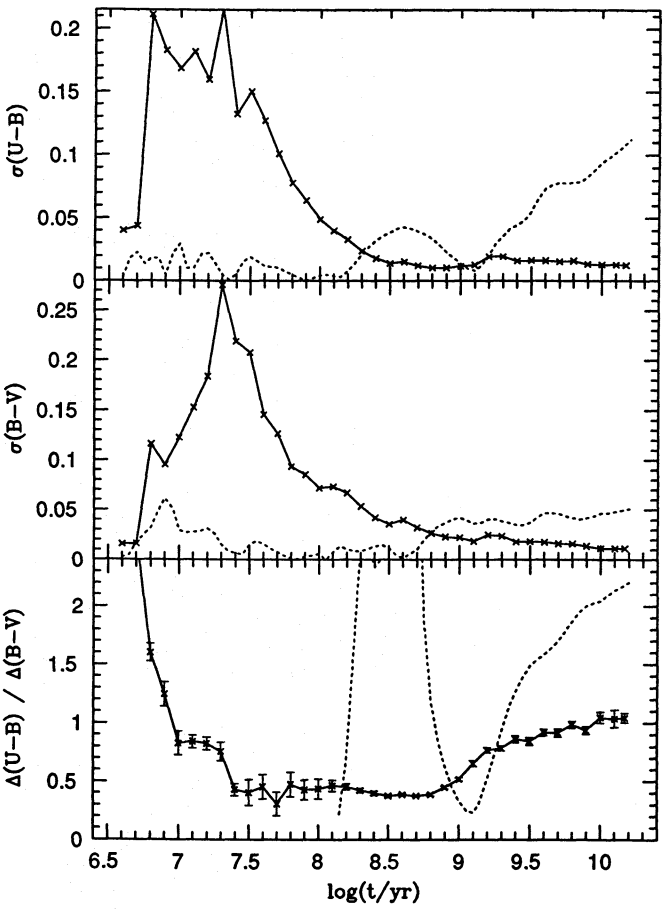

Fig. 6. The time dependence of the average deviations around the mean colors due to stochastic effects, $\sigma(B-V)$ and $\sigma(U-B)$, for a set of models with $Z = 0.008$ and $M_V = -6$ (crosses and continuous line). The bottom panel presents the slope of the dispersion in the $(U-B)$ vs. $(B-V)$ diagram, $\Delta(U-B)/\Delta(B-V)$, together with the corresponding error bars. The dotted line in each panel shows the mean differences in colors for models with metallicities differing by ± 0.2 dex from that of the reference case $Z = 0.008$

4.2. *Other causes of color dispersion*

Possible variations of the metallicity and reddening from cluster to cluster, and photometric errors in the magnitudes and colors of individual clusters, concur to scatter the integrated colors.

Dispersion in metallicity among coeval clusters. The young and intermediate-age clusters in the Olszewski et al. (1991) catalog have metallicities ranging from [Fe/H] $= 0 \pm 0.2$ to [Fe/H] $= -0.7 \pm 0.2$ thus suggesting an intrinsic dispersion of at least σ([Fe/H]) ~ 0.2 dex. Similar estimate was derived by Frogel et al. (1990) from the color distribution of M stars in clusters with age of ~ 1 Gyr.

The effect of the metallicity dispersion on the integrated UBV colors can be easily evaluated by comparing the colors of SSPs with different metallicity. This is shown by the dotted lines in the three panels of Fig. 6 displaying $\sigma(B-V)$, $\sigma(U-B)$ and $\alpha = \Delta(U-B)/\Delta(B-V)$ for SSPs with metallicity varied by 0.2 dex with respect to the reference value $Z = 0.008$.

It turns out that for ages younger than $\log t = 8.0$, a dispersion in metallicity has little effect on the colors as compared to those by stochastic effects (at least for $M_V = -6$). On the contrary, at ages older than $\log t = 8.4$ for $U-B$ and $\log t = 8.8$ for $B-V$, the color dispersion caused by the metallicity dispersion overwhelms that caused by the stochastic effects. As a consequence of this, in the red part of the $(U-B)$ vs. $(B-V)$ diagram the mean slope of the dispersion gets steeper than in the case with the sole effects of stochastic nature in the IMF.

Dispersion in reddening among coeval clusters. The $E(B-V)$ data by Persson et al. (1983) indicate the existence of an intrinsic dispersion of about $\sigma[E(B-V)] \simeq 0.05$ in the reddening across the LMC. This is an important source of color dispersion only for ages older than $\log t \sim 8.5$. The slope of the reddening vector is $\Delta(U-B)/\Delta(B-V) = 0.72$.

Photometric errors. Figure 2 in Bica et al. (1992) indicates that in BCDSP data the mean internal photometric errors are lower than ~ 0.05 mag in $B-V$ and $U-B$ colors for clusters with $V \simeq 13$. For clusters brighter than $V = 12$, the uncertainties in the colors caused by photometric errors are negligible with respect to those induced by the other effects discussed above. Another source of uncertainty is related to the contamination of the cluster colors by the surrounding field stars. This kind of uncertainty is, however, difficult to evaluate. Probably it is negligible for the majority of clusters, being significant only for those lying in regions with highly non-uniform background. As far as the possibility of bad sampling of cluster stars is concerned – i.e. some bright stars belonging to a cluster falling outside the diaphragm used in the photometric survey –, this is less of a problem because its effect likely mimics that of stochastic fluctuations in the IMF. Therefore, photometric errors are expected to concur with the other sources of color dispersion only in the case of the faintest clusters ($V \gtrsim 13$) with age older than $\log t \sim 8.0$.

To summarize the above discussion, in magnitude limited samples of UBV data, stochastic effects dominate the color dispersion of the young clusters, whereas those by reddening+metallicity (and perhaps photometric errors) probably dominate the color dispersion of the clusters older than $\log t \sim 8.5$.

5. Analysis of the observational data

Before comparing the theoretical colors with the UBV data, we shortly describe the BCDSP catalog, as its final version is not yet published. The catalog contains 624 objects, a few of which with previous precise photometry by other authors. The clusters observed by BCDSP (the bulk of the catalog) are selected one-by-one by means of a careful analysis of the ESO/SERC Survey plates, together with the measurement of their aperture size and the choice of the comparison field. Arguments are given in Bica et al. (1992) showing that the sample is complete down to the integrated magnitude $V = 13.2$, as indicated by the fall-off occurring at this magnitude in the luminosity function (LF) of the clusters in the LMC Bar.

The catalog contains more than 100 observations of stellar aggregates inside H II regions. Many of these objects cannot be clearly classified as clusters (i.e. gravitationally bound systems). Moreover, the contamination by gas emission makes uncertain the interpretation of their UBV colors in terms of the evolution of the component stars. Fortunately, most of these objects are located in a distinct region of the $(U-B)$ vs. $(B-V)$ diagram: indeed they all fall in the area of the E-SWB group 0 defined by BCDSP, namely the region bounded by $B-V < 0.0$ and $U-B \lesssim -0.7$. We prefer to keep these data in our list, but care will be paid when interpreting their UBV colors.

5.1. Analysis of the $(U-B)$ vs. $(B-V)$ plane: effects of color dispersion

The data of BCDSP has been already presented in the two-color planes of Figs. 4 and 5, together with the color evolution of SSPs. Although the agreement between the gross features of the SSPs and observational data is remarkably good, the detailed comparison requires that both the history of metal enrichment in the LMC and scatter in the colors induced by the various causes previously discussed are taken into account.

To this aim, we plot in the theoretical $(U-B)$ vs. $(B-V)$ plane of Fig. 7 both the color evolution of Models A and B of chemical enrichment and the simulations of individual clusters of different age and metallicity.

The cluster simulations obey the same law of metal enrichment as Model A and B and include the effects of color dispersion due to stochastic effects. 50 synthetic clusters are calculated at ages spaced by $\Delta\log t = 0.1$, and for total magnitudes $M_V = -6$ for $\log t > 8.0$ and $M_V = -7$ for $\log t \leq 8.0$. This age dependence for the total magnitude M_V approximately mimics the trend shown by the faintest clusters in BCDSP sample, whose total magnitudes are seen to increase with the age (see also the data displayed in Fig. 13 below).

In addition to this, for each value of the age, Models A and B are also calculated with metallicities differing by ± 0.3 dex from the nominal values given by equations (1) and (2). This gives an idea of the maximum color dispersion induced by a scatter in metallicity among coeval clusters.

The $(U-B)$ vs. $(B-V)$ plane of Fig. 7 clearly illustrates the effects induced on the colors by the law of metal enrichment and, separately, the amounts of dispersion induced by stochastic effects and metallicity variations. Finally, we introduce two arrows in the figure that schematically illustrate the total effect of color dispersion for clusters with ages $\sim 10^8$ and 10^9 yr, when all the sources of color dispersion are added together. It is clear that the total effect of color dispersion occurs along well-defined directions according to the position in the $(U-B)$ vs. $(B-V)$ diagram. We refer to this direction as the *mean dispersion vector*.

For the young clusters, i.e. bluer than $B-V = 0.4$, the amount of spread due to stochastic effects well reproduces the scatter observed in Fig. 4. In addition to this, the very young clusters seem to present a bimodal distribution of colors (see Fig. 7): a first group bluer than $B-V = -0.1$ and a second

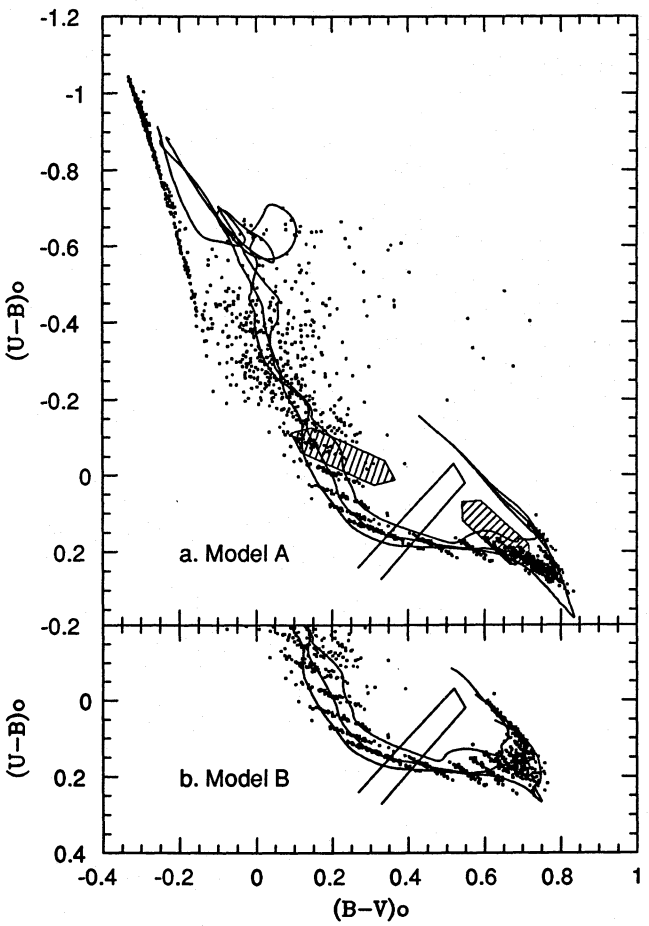

Fig. 7. (Panel **a**): The color evolution of Model A with the nominal AMR of Eq. (1) and similar models in which at any age the metallicity differs by ±0.3 dex (solid lines). They show the effects of dispersion in metallicity. Superimposed are the colors of synthetic clusters (dots) obeying the age-metallicity relation of Model A. At each value of the age (spaced by $\Delta \log t = 0.1$) 50 simulations are shown, clearly showing the effect of stochastic fluctuations in the IMF. See the text for more details. The shaded arrows schematically illustrate the total effect of dispersion, at ages $\sim 10^8$ and 10^9 yr, when all the factors are added together. The area in the box corresponds to the gap identified by BCDSP (see Fig. 5). Notice how the upper part of the area is not filled by clusters. (Panel **b**): The same as in (Panel **a**) but for the AMR of Model B

group stretching up to $B - V = 0.7$. The dichotomy arises from the very small number of RSG stars present in each cluster with $M_V = -7$ (typically 0 to 2 RSGs) that induces a large separation in color between clusters with and without RSGs (see GB93). The simulations of Fig. 7 seem to overestimate this effect with respect to the observed distribution of Fig. 4. However we notice that the bulk of the very young clusters in the BCDSP sample are brighter than $M_V = -7$, and thus have a number of RSGs per cluster high enough to make them populate the region comprised between these two extreme cases. Moreover, differential reddening probably scatters the clump of young, very blue clusters (those without RSGs) towards redder colors.

As far as red clusters are concerned, the history of metal enrichment plays the key role in determining their distribution in the two-color plane, as shown by the evolution of Models A and B. Stochastic effects are not enough to account for the observed scatter in the colors, and the additional contributions due to the dispersion in reddening (~ 0.05 mag in $B - V$) and metallicity seem to be required.

5.2. Is there any evidence of an age gap from the $(U - B)$ vs. $(B - V)$ plane ?

The study by Olszewski et al. (1991) shows that a dichotomy in the distribution of metallicities and ages for LMC clusters is likely to exist. In fact, young and intermediate-age clusters (E-SWB types I–VI) have metallicities in the range $0.0 >$ [Fe/H] > -0.7, while old clusters (E-SWB type VII) have $-1.7 <$ [Fe/H] < -2.2. Furthermore, all the E-SWB VII clusters with observed CMDs are older than 12 Gyr, while young and intermediate-age clusters evenly span the age range from a few Myr to $\simeq 3$ Gyr. No clusters, with the exception of ESO 121SC03, are found to have ages in the 3 – 12 Gyr interval (Da Costa 1991).

In order to check whether any evidence of the above dichotomy can be found in the $(U - B)$ vs. $(B - V)$ diagram, let us examine the color evolution of Models A and B in Fig. 5. To this aim, it must be recalled that Models A and B describe the locus along which ideal clusters of different age and metallicity would exist.

If chemical enrichment in the LMC obeys Model A, the observational age gap corresponds to the portion of the evolutionary path red-ward of $B - V = 0.8$, where indeed very few (and faint) clusters are seen. It follows that the age gap is not at variance with the observed distribution of clusters in the $(U - B)$ vs. $(B - V)$ plane. This is even more true considering that the various causes of color dispersion would blur the path of Model A in this region (see panel a of Fig. 7) and give rise to even redder clusters that are not observed.

On the contrary, if chemical enrichment obeys Model B the theoretical path would run across the data over the entire age interval. This could be considered at variance with the observational gap. However, it must be noticed that the age interval $3 < t < 12$ Gyr (gap) corresponds to the portion of the Model B curve with $B - V \simeq 0.77$ and from $U - B = 0.21$ to $U - B = 0.12$, partially overlapping the range of $U - B$ colors of the very old clusters ($U - B \lesssim 0.18$). Therefore the age gap translates into a color gap of about $\Delta(U - B) = 0.03$, which is very difficult to detect also considering the natural dispersion of the colors. Also in this case, the age gap is not in contrast with the observed distribution of clusters in the $(U - B)$ vs. $(B - V)$ plane.

5.3. The van den Bergh gap in the $B - V$ histogram

Since the early study by van den Bergh (1981) showing the presence of a gap, approximately 0.3 mag wide and centered at about $B - V \sim 0.5$ in the $B - V$ histogram, the subject has

been addressed by several authors with contrasting conclusions. Among others we recall the following explanations:

1) The so-called phase transitions, which stand on the notion that fast changes in the integrated colors occur at the ages in which both AGB and RGB stars develop in a SSP for the first time (Renzini & Buzzoni 1986). However, the study of Bressan et al. (1994) on the theory of population synthesis clarifies that neither the appearance of the AGB nor of the RGB stars can generate appreciable changes in UBV colors. In particular, they show that the effects on colors caused by the appearance of RGB stars in a SSP are always masked by the already existing AGB stars, so that no variation in the integrated colours is produced (see also CBB88). On the observational side, the works by Corsi et al. (1994) and Ferraro et al. (1994) indicate that the change in $B-V$ colors is not driven by RGB or AGB stars. These considerations seem to rule out the possibility that these features were responsible for the gap.

2) An effect of the varying extension of the blue loop of CHeB stars, which progressively shifts to the red and eventually merges the red clump near the Hayashi line as the clusters get old. Battinelli & Capuzzo-Dolcetta (1989) suggested that this feature of the stellar models, together with the RGB phase transition, provide the most plausible explanation of the gap. This is at variance with the observation showing that clusters with integrated colors $B-V \sim 0.4$ exist which have the CHeB phase already concentrated in a red clump. As examples we have NGC 1831, NGC 1868 and NGC 2249 (see CMDs from Corsi et al. 1994).

3) An idea subtly introduced by Frenk & Fall (1982) according to which the gap simply results from color degeneracy. More precisely, the concentration of clusters bluer than the gap is caused by the relatively small range of $B-V$ colors spanned by these, whereas the concentration of clusters redder than the gap is caused by the fact that the intermediate age clusters of normal metallicity and the old, low-metallicity ones have similar $B-V$ colors. Therefore, when they are projected onto a $B-V$ histogram, a bimodal distribution of colors results, even if the clusters equally populate the evolutionary sequence.

4) The suggestion advanced by CBB88 that the gap in the $B-V$ histogram results from the combined action of a normal sequence of cluster colors incorporating an age-metallicity relation and a particular ADF. While the former sets the position of the gap, the latter determines the number ratio between blue and red clusters.

In Fig. 8 we present the histogram of the $B-V$ colors from the BCDSP sample. It can be noticed that the gap is not as pronounced as in van den Bergh (1981). The main reason for it is that the BCDSP sample includes a significant number of faint clusters, for which there was not previous photometry, that now fall into the color gap. In this context, we would like to remark that the seven young clusters with $B-V > 0.4$ and $U-B < -0.3$ (see Fig. 4) have not been included in the histogram.

In order to single out the physical cause of the color gap, we derive the theoretical distribution of $B-V$ colors using the method outlined by Battinelli & Capuzzo-Dolcetta (1988).

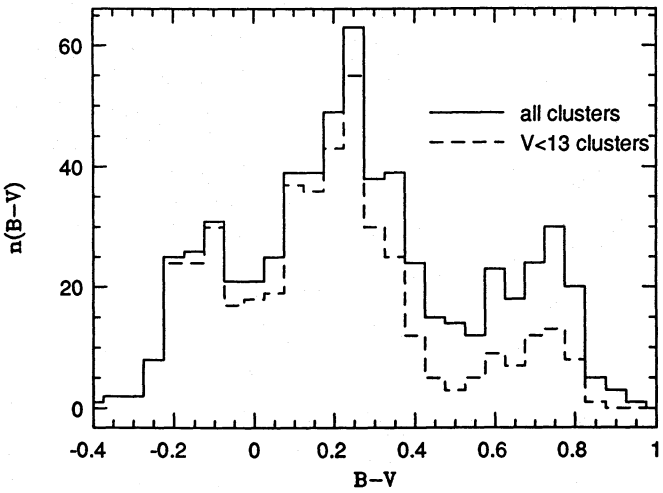

Fig. 8. Observed $B-V$ histogram from the BCDSP data, showing either all clusters or only those with $V < 13$. It is worth recalling that for $B-V < 0$ the sample contains a significant number of associations

With any model of color evolution, $(B-V)(t)$, the distribution of clusters in the $B-V$ color $f(B-V)$ is given by

$$f(B-V) = f(t)\ |\mathrm{d}(B-V)/\mathrm{d}t|^{-1} \qquad (4)$$

where $f(t)$ is the ADF for the clusters in the sample. Equation (4) does not include effects of color dispersion caused by the finite number of stars per cluster.

As the color derivative $\mathrm{d}(B-V)/\mathrm{d}t$ can present a series of near-zero and negative values (e.g. during the loop of the RSG phase), synthetic $B-V$ histograms are generated by integrating $f(B-V)$ over equally spaced intervals of $B-V$, and summing up all the contributions to each interval from different parts of the evolutionary curve under consideration.

Defined this procedure, in order to check the effect of different ADFs, we calculate a series of synthetic $B-V$ histograms for several functions $f(t)$, using the color evolution $(B-V)(t)$ of Models A and B. Three typical cases are considered: **(a)** a sample of clusters with constant ADF, $f(t)$ = constant; **(b)** a sample of clusters with ages evenly distributed in $\log t$, i.e. $f(t) \propto t^{-1}$; **(c)** a sample of clusters with the ADF of Galactic open clusters given by Wielen (1971). The results are shown in Fig. 9.

A bimodal distribution of colors is obtained in all cases, however the amplitudes of blue and red peaks depend very much on the assumed $f(t)$. Specifically, cases (a) and (c) predict too many red and blue clusters, respectively, whereas case (b) roughly produces the number ratio of red to blue clusters observed in the LMC (see CBB88 for a similar conclusion). The discussion below will mainly refer to this paradigmatic case.

The results shown in Fig. 9 lend support to the interpretations of Frenk & Fall (1982) and CBB88 at the same time. Indeed, the bimodal distribution of $B-V$ colors is produced by the existence of two major changes in the slope of the UBV evolutionary path of an ensemble of clusters whose metallicity

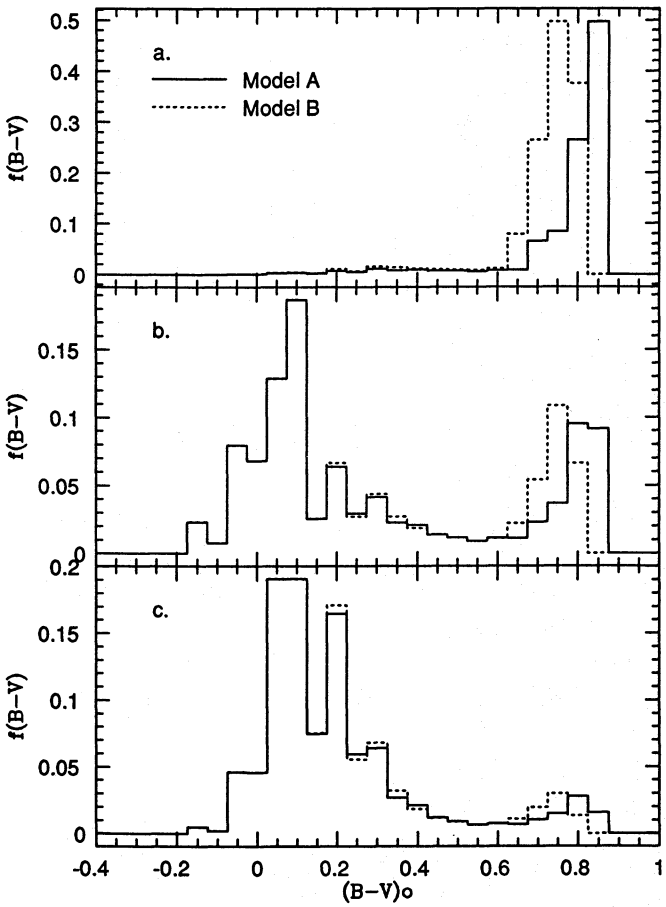

Fig. 9a–c. Synthetic $B-V$ histograms for three different $f(t)$ distributions and the $(B-V)(t)$ curves of Models A and B. The following cases are shown: (Panel **a**) a sample of clusters with constant distribution of ages, $f(t)$ = constant, (Panel **b**) a sample of clusters evenly distributed in $\log t$, i.e. $f(t) \propto t^{-1}$, (Panel **c**) a sample with the same age distribution as that of Galactic open clusters given by Wielen (1971)

increases toward the present (for instance like Models A and B). The changes in question are:

1) The first at $(B-V)_0 \sim 0.3$, which occurs when the upper MS is populated by A0 stars. It turns the $B-V$ color evolution from almost-constant to linearly-increasing with $\log t$ (see Sect. 2.1), and causes an increase in the $\mathrm{d}(B-V)/\mathrm{d}t$ derivative and hence a minimum in $f(B-V)$ at $B-V \sim 0.5$.

2) The second at $B-V \sim 0.8$, which bends the evolutionary path to bluer colors. This happens when the metallicity is low enough to generate the hook-like feature described in Sect. 3. It causes a degeneracy in $B-V$ colors between intermediate-age metal-rich clusters and old metal-poor ones, at $B-V \gtrsim 0.6$.

Furthermore, the detailed shape of the $B-V$ histogram depends very much on the adopted $f(t)$ as clearly demonstrated by the results shown in panels (a), (b), and (c) of Fig. 9. Limiting the discussion to case of panel (b) which goes closer to the observational $B-V$ histogram (see Fig. 8), even if the theoretical distribution matches the color of the minimum ($B-V \sim 0.5$), it cannot reproduce the details of the observational one. In particular we notice two differences: a) On the side of the blue clusters, the theoretical distribution peaks at $(B-V)_0 = 0.1$, whereas the observed one peaks at $B-V = 0.3$ (reddening cannot be a solution). b) On the side of the red clusters, the theoretical distribution shows a pronounced maximum (especially for Model A) at the reddest colors [$(B-V)_0 \simeq 0.8$], which is absent in the data.

How can we solve the above discrepancy? Two important results of our analysis provide useful constraints: a) the positions of the blue and red peaks are insensitive to the slope of the age distribution function $f(t)$ (cf. Fig. 9); b) the theoretical color evolution $(B-V)(t)$ agrees with the data (cf. Figs. 4 and 5). Therefore, drastic modifications to $f(t)$ other than changes in the slope are unavoidable. We will argue in Sect. 8.4 that bursts of cluster formation at suitable epochs lead to a better agreement between theory and observations.

In addition, we note that stochastic effects (and to a smaller extent variations in the reddening and metallicities of individual clusters) blur the distribution of $B-V$ colors. However, based on the results of Sect. 5.1, we can conclude that the effect in the $B-V$ histogram is small for clusters redder than $B-V \simeq 0.4$ (and hence relatively old), and noticeable only for the bluest (and hence youngest) clusters. In any case, the amount of color dispersion is not enough to significantly populate the region of the gap.

5.4. The BCDSP gap in the $(U-B)$ vs. $(B-V)$ diagram

BCDSP noted that their data exhibited a clear gap in the $(U-B)$ vs. $(B-V)$ diagram, approximately 0.1 mag wide in both colors, centered at $U-B \simeq 0.19$ and $B-V \simeq 0.47$. It is represented in Fig. 5 as a strip in which only two clusters (SL 276 and NGC 1861) are contained. It was firstly interpreted as being produced by the RGB phase transition predicted by Renzini & Buzzoni (1986). Once again, this explanation in terms of the RGB phase transition disagrees with the results of theoretical models of SSPs (see Sect. 5.3).

We recall that the arguments in favour of this interpretation (Bica et al. 1991) stand on the analysis by Buonanno et al. (1988), which reported the possible presence of the RGB in the CMD of NGC 1987, a cluster located exactly at the bottom red border of the gap. However, in a more recent paper, Corsi et al. (1994) conclude that the RGB seen in the CMD of NGC 1987 in reality belongs to the crowded field surrounding the cluster. Moreover, two additional clusters located at the red of the gap, NGC 2209 and NGC 2108, according to the latter authors do not show evidence of an extended RGB[1]. It makes very improbable that the gap could be interpreted in terms of the appearance of the RGB in the clusters.

What could be the cause of the gap in the $(U-B)$ vs. $(B-V)$ diagram, if not an evolutionary effect at a particular age?

[1] The bluest cluster clearly showing the RGB is NGC 2190. It has $B-V = 0.63$, which coincides with the color at which the RGB is expected to appear according to our models (see Fig. 5, and the photometric data from Table 3)

In the following we suggest that the gap originates from the subtle combination of the effects of color dispersion superposed to the natural age-metallicity evolution involved in a sample of clusters of any age.

The hint comes from the comparison of Fig. 5 with Fig. 7. We call attention to the following: First of all, in Fig. 5 the evolutionary paths of Models A and B (which in a simple fashion take the AMR of the LMC into account) cross the region of the gap in a single point coincident with the position of SL 276 and NGC 1861, and in general go *beneath and around* the region of the gap which is actually void of clusters. Second, the color dispersion illustrated in Fig. 7 acts in different fashions along the evolutionary path. For clusters in the same range of $B-V$ color as that of the gap, the mean dispersion vector is parallel to the evolutionary path, so that no (or very small) scatter of the colors occurs. At bluer and redder $B-V$ colors the slope of the mean dispersion vector differs from that of the evolutionary path, so that a significant scatter of the colors is produced. The result is a region of the color-color diagram which is void of clusters, which corresponds to upper corner of the BCDSP gap (see Fig. 7).

Accordingly, the interpretation follows that the young clusters scattered toward the red define the blue side of the gap, whereas the intermediate-age and old clusters scattered toward the blue define the red side of it. The gap is nothing else but a region of the $(U-B)$ vs. $(B-V)$ plane confined between the maximum red-ward scatter of the blue clusters and the maximum blue-ward scatter of the red ones belonging to the hook caused by the age-metallicity relation. Were this missing, the formation of the gap would not have been possible. No peculiar properties of the stellar models are needed to explain this feature of the $(U-B)$ vs. $(B-V)$ diagram.

However, the reader can also notice in Fig. 5 that the gap region is also characterized by having a small density of clusters along the evolutionary sequence. We will return to this point in Sect. 8.4.

6. Age calibration

The full understanding of the information contained in the color distribution of our sample of clusters requires the correct determination of the age distribution $f(t)$, and in turn the calibration of the cluster ages by means of an independent method. This will be the subject of this section, where we derive the ages for a group of template clusters.

Instead of searching for ages in the literature, we prefer to collect a sample of good quality CMDs, for which we re-derive the ages using the library of isochrones of Bertelli et al. (1994). In this way we can avoid a problem present in several previous studies, i.e. that of heterogeneity in the way cluster ages are determined.

6.1. The color-magnitude diagrams and metallicities

The criteria for the selection of CMDs are:

- CCD data only (which limits the search in the literature to the last $\sim$ 10 years).
- Calibrated data in Johnson's BV pass-bands.
- Good photometric quality, i.e. evaluation of crowding and field contamination.

Table 1 presents the collected data, in order of increasing TAMS magnitude.

From the CMDs we derive three characteristic loci (magnitudes) to be used as age-indicators: the MS-termination, $V_{\rm TAMS}$; the faintest limit of the red giant stars, $V_{\rm RGf}$, supposed to be at the stage of CHeB; and the brightest red giants (most likely AGB stars), $V_{\rm RGb}$ (see Table 1). In the case of the clusters with a red clump, for which the contamination by field red giants is considerable, the mean magnitude of the clump is used instead of that of the faintest red stars.

All relevant data are presented in Table 1, together with previous determinations for the reddening and metallicity. In those cases for which no reference for $E(B-V)$ is found, the mean value across the LMC $E(B-V)=0.07$ from the Burstein & Heiles (1984) maps is used. Throughout this work, the LMC distance modulus is assumed to be $(m-M)_0=18.5$ (Panagia et al. 1991; Bertelli et al. 1993).

While the determinations of the color excess by different authors are in satisfactory mutual agreement, those for the metallicity greatly differ. This can be seen looking at the data compiled by Elson (1986) and Seggewiss & Richtler (1989), who collected from the literature metallicity determinations obtained from different methods (e.g. Walraven, Washington and DDO photometry, spectroscopy, previous CMDs, etc).

There is just one homogeneous and recent compilation of metallicities for a significant number of LMC clusters, namely the list of Olszewski et al. (1991), which contains data for 70 red clusters whose [Fe/H] determinations have a 0.2 dex accuracy. However, their metallicities for young and intermediate-age clusters are systematically larger than previous spectroscopic determinations of Cohen (1982) and Cowley & Hartwick (1982). Given the quality and internal consistency of Olszewski et al.'s analysis, we prefer to use their [Fe/H] values for the clusters in their list, and adopt the value -0.4 ($Z=0.008$) for all the others but for two exceptions in which the metallicity was taken from the source of the CMD.

Due to this particular selection of the metallicities, only half of the clusters have individual [Fe/H] determinations (mainly the red ones). Fortunately the chief age indicators used in this work – namely, the magnitudes of the TAMS and red CHeB stars – do not depend very much on the metallicity.

6.2. The isochrones and age calibration

Bertelli et al.'s (1994) library of isochrones provides the age-calibrations for the magnitudes of the TAMS $M_{V\,\rm TAMS}$, the mean locus of red CHeB stars $M_{V\,\rm CHeB}$ (just at the start of central He-burning), and the AGB-tip $M_{V\,\rm AGB}$. A few comments are worth:

The first two age indicators weakly depend on metallicity. $M_{V\,\rm TAMS}$ is a useful age-indicator over a large range of ages, from $\log t = 6.6$ to 10.2 (ages are in years). The slope of the

Table 1. The sample of template clusters with published CMDs

Cluster	$V_{\rm TAMS}$	$(B-V)_{\rm TAMS}$	$V_{\rm RGf}$	$V_{\rm RGb}$	$E(B-V)$	[Fe/H]	References	Comments
NGC 1850A	13.0	−0.1	–	–	0.18	−0.4	12,12,12	a
NGC 1858	13.2	−0.25	–	–	0.15	−0.4	12,12,12	a
NGC 2004	13.5	−0.15	13.5	12.8	0.09	–	9,1,no	c
NGC 2100	14.3	0.0	14.0	13.0	0.19	–	9,1,no	e
NGC 1711	15.7	−0.12	15.0	13.4	0.14	–	9,1,no	c,d
NGC 2164	16.0	−0.1	16.5	15.0	0.09	−0.7	10,10,10	
NGC 2214	16.2	−0.07	15.0	14.4	0.07	–	9,1,no	f
NGC 1850	16.2	−0.1	15.7	14.3	0.18	−0.4	12,12,12	b
NGC 1866	16.6	0.0	16.7	15.5	0.07	∼0.0	2,2,2	h
NGC 2010	16.9	−0.02	16.7	15.3	0.07	–	4,no,no	g
NGC 2134	17.1	0.06	17.5	15.5	0.25	−0.4	13,13,13	
NGC 1756	17.6	0.02	17.3	16.5	0.07	–	3,no,no	
NGC 2107	18.0	0.15	17.5	17.2	0.19	–	3,8,no	
NGC 1831	18.2	0.05	18.4	16.5	0.05	+0.01	11,11,7	i
NGC 2249	18.5	0.24	19.0	17.4	0.25	−0.4	13,13,13	i
NGC 1987	18.8	0.18	19.2	16.2	0.12	–	3,1,no	i
NGC 2108	19.1	0.20	19.3	16.4	0.18	–	3,8,no	i
NGC 1868	19.3	0.15	19.3	16.8	0.07	−0.50	3,8,7	i
NGC 2190	19.5	0.20	19.5	17.0	0.07	−0.12	3,no,7	i,j
NGC 2209	19.5	0.25	19.7	16.6	0.07	–	3,8,no	i
NGC 2162	19.6	0.25	19.2	16.2	0.07	−0.23	3,8,7	i,j
NGC 2173	20.0	0.40	19.1	16.3	0.07	−0.24	3,8,7	i,j
LW 79	20.3	0.43	19.4	16.8	0.08	−0.50	5,5,7	i,j
H 4	20.5	0.42	19.0	17.7	0.07	−0.15	6,6,7	i,j

References column refer to the source of CMD, $E(B-V)$ and [Fe/H] data respectively: 1) Cassatella et al. (1987); 2) Chiosi et al. (1989); 3) Corsi et al. (1994); 4) Mateo (1988a); 5) Mateo & Hodge (1987a); 6) Mateo & Hodge (1987b); 7) Olszewski et al. (1991); 8) Persson et al. (1983); 9) Sagar et al. (1991a); 10) Vallenari et al. (1991); 11) Vallenari et al. (1992); 12) Vallenari et al. (1994b); 13) Vallenari et al. (1994a). A "no" means that the default values $E(B-V) = 0.07$ and [Fe/H] = −0.4 are adopted.
Comments: a) No RSG is present in this cluster. b) Do not include very young MS of NGC 1850A. c) The TAMS is not clearly separated from blue giants. d) $V_{\rm RGb}$ is defined by a single red star; the brightest blue giants are at $V \simeq 14.0$. e) The blue stars are distributed atop the MS up to $V = 12.0$, but certainly these bright stars are core He-burners, as the RSGs are at $13.0 < V < 14.6$. The TAMS ought to be between 13.5 and 15.0, and the value 14.3 was assumed. f) This cluster apparently has a double loop of evolved stars. The value $V_{\rm RGf}$ has been taken at what seems to be the lowest envelope of the brighter loop. g) The $V_{\rm RGb}$ is defined by a single red star. The brightest blue giants are clumped between 16.7 and 15.9. h) According to Chiosi et al. (1989), the brightest red giants, at $V = 15.0$, are probably field population. i) Cluster with the CHeB stars in a red clump. j) Cluster with a developed RGB.

curve $M_{V\,\rm TAMS}(\log t)$ is ~ 0.33, and thus an uncertainty in the observed TAMS magnitude of about 0.3 mag (a reasonable estimate for most of the CMDs for old clusters) would reflect into an uncertainty of 0.1 in $\log t$. This is a considerable source of error, but less of a problem when compared to other uncertainties to be discussed below. Furthermore, uncertainties in metallicity give rise to uncertainties in the age not exceeding 0.1 in $\log t$.

$M_{V\,\rm CHeB}$ uniquely determines the age up to $\log t = 8.5$. In older clusters, the CHeB phase proceeds at almost constant magnitude, and $M_{V\,\rm CHeB}$ is no longer a useful age-indicator. Nevertheless, it can be applied up to ages of $\log t = 8.9$, provided that the TAMS magnitude ensures that the cluster is younger than this limit. For ages $\log t < 6.8$, severe mass loss by stellar wind prevents the appearance of evolved red stars, and in this case the only available age-indicator is $M_{V\,\rm TAMS}$.

For clusters older than $\log t \simeq 8.0$, $M_{V\,\rm AGB}$ is a good age indicator, however very sensitive to metallicity. Another problem is that even in a rich cluster, the number of stars expected at the AGB-tip is very small, so that the luminosity of the brightest objects provides only a lower limit to the real AGB-tip and therefore older ages could be erroneously assigned.

We use these relations in order to assign ages to the clusters listed in Table 1. The results are given in Table 2; for each cluster we present the three age estimates $\log t(M_{V\,\rm TAMS})$, $\log t(M_{V\,\rm CHeB})$ and $\log t(M_{V\,\rm AGB})$, the adopted mean age $\overline{\log t}$, and the adopted values for [Fe/H]. The entries marked with a colon (:) are those for which the adopted [Fe/H], and consequently $\log t(M_{V\,\rm AGB})$, are uncertain.

6.3. Comments on individual clusters

NGC 1711 (Sagar et al. 1991a) presents a RSG clump at $V = 15.0$, much more evident than the MS-termination (there are blue stars up to $V = 14.0$). However, the number of blue

Table 2. Ages for the sample of template clusters of Table 1

Cluster	$\log t$ from M_V of TAMS	CHeB	AGB	mean	[Fe/H]
NGC 1850A	6.82	–	–	6.82	−0.4:
NGC 1858	6.88	–	–	6.88	−0.4:
NGC 2004	6.99	7.66	–	7.33	−0.4:
NGC 2100	7.10	7.71	–	7.40	−0.4:
NGC 1711	7.58	7.99	–	7.79	−0.4:
NGC 2164	7.72	8.27	7.95	7.99	−0.7
NGC 2214	7.81	8.03	7.75:	7.92	−0.4:
NGC 1850	7.70	8.09	7.59:	7.90	−0.4:
NGC 1866	7.96	8.32	7.96:	8.14	−0.4:
NGC 2010	8.07	8.32	8.09:	8.19	−0.4:
NGC 2134	7.94	8.36	7.96	8.15	−0.4
NGC 1756	8.33	8.42	8.73:	8.38	−0.4:
NGC 2107	8.34	8.39	8.85:	8.37	−0.4:
NGC 1831	8.61	8.59	8.23	8.60	+0.01
NGC 2249	8.50	8.58	8.82	8.54	−0.4
NGC 1987	8.68	8.84	8.39:	8.76	−0.4:
NGC 2108	8.72	8.81	8.40:	8.77	−0.4:
NGC 1868	8.87	–	8.98	8.87	−0.50
NGC 2190	8.91	–	8.63	8.91	−0.12
NGC 2209	8.96	–	9.15:	8.96	−0.4:
NGC 2162	8.95	–	8.33	8.95	−0.23
NGC 2173	9.06	–	8.38	9.06	−0.24
LW 79	9.16	–	8.93	9.16	−0.5
H 4	9.15	–	9.12	9.15	−0.15

stars clearly drops for $V < 15.7$, which is taken as the MS-termination.

NGC 2004 (Sagar et al. 1991a) shows a well-defined RSG clump at $13.0 < V < 13.5$, and a sequence of blue stars terminating abruptly at $V = 13.5$. If $V_{\rm TAMS} = 13.5$ is taken as the MS-termination, a huge difference arises between the ages from the TAMS and the RSG stars ($\Delta \log t \sim 0.6$). Most of the age discrepancy would be removed if the TAMS is taken at $V = 14.3$ (where there are two MS stars slightly shifted to the red); but in this case it would be difficult to interpret the brightest blue stars as stars in the Cepheid loop, just because they are fainter than the RSGs.

NGC 2100 (Sagar et al. 1991a) is similar to NGC 2004 in the sense that there is a RSG clump and the MS-termination is not well defined (could be anywhere between $V = 13.5$ and 15.0). Therefore, the choice of $V_{\rm TAMS} = 14.3$ is uncertain. Independently of the exact location of the TAMS, there seems to be a too large number of BSGs, some as bright as $V = 12$. Although there are two RSGs fainter than $V = 14.0$, the RSG stars crowd the region between $V = 13.4$ and 14.0. The same problem as for NGC 2004 occurs. There is a large difference between the age estimated from the red and the blue stars.

NGC 2164 (Vallenari et al. 1991; Sagar et al. 1991a) has both the MS-termination and the RSG clump sharply defined.

NGC 2214 (Sagar et al. 1991a) is a double cluster containing two sequences of RSGs. It is interpreted as being formed by the merger of two clusters with different ages (Sagar et al. 1991b). The age assignment is less of a problem because the younger RSG clump is clearly defined by 5 stars at ($V \simeq 15.5, B - V \simeq 1.3$). Although there is a single red star at $V = 13.3$, the brightest red stars are concentrated up to $V = 14.4$. The TAMS is also clearly defined.

NGC 1858 (Vallenari et al. 1994b) does not contain evolved red stars, and thus the TAMS is the only available age indicator.

NGC 1850 (Vallenari et al. 1994b) is made of two main groups of stars: a very young generation of massive stars (NGC 1850A; notice that in the Vallenari et al. paper it is indicated as Region B), which appears as a thin MS departing from the bulk MS at $V \sim 16.5$ and extending up to $V = 13.0$ (see Fig. 3 in Vallenari et al. 1994b), and the older main body (Region A in Vallenari et al. 1994b). In the CMD of this latter, the magnitudes of the TAMS and RSG clump are clearly defined.

NGC 1866 (Chiosi et al. 1989), *NGC 2010* (Mateo 1988a), *NGC 2134* (Vallenari et al. 1994a). In these clusters there is no difficulty in defining the MS-terminations, the faintest and the brightest red stars, because the contamination by field stars, which is already important at these magnitudes, is properly taken into account. However, there is the systematic discrepancy between the ages derived from $V_{\rm RGf}$ and those from $V_{\rm TAMS}$. The former are about $\Delta \log t = 0.3$ older than the latter. In order to rule out this discrepancy, the magnitude difference between the red giant stars and the TAMS should be lowered by about ~ 1.0 mag. Clearly, photometric errors cannot be responsible for this difference, as they do not exceed $\simeq 0.25$ mag in each case.

Remaining clusters. The majority of these clusters is from the sample studied by Corsi et al. (1994), so that the data are highly homogeneous. The CHeB phase is concentrated in a red clump, whose magnitude is easily determined. For the clusters younger than NGC 1868, the corresponding CHeB magnitude contains already some dependence on the age, and age estimates from the CHeB magnitude agree with those from the TAMS. For clusters older than NGC 2190 the ages are based only on the TAMS, and are affected by a slightly larger uncertainty due to photometric errors and field contamination.

6.4. Other comments on ages

Looking at the entries of Table 2, we see that the ages determined from the faintest red giants in general agree with those obtained from the TAMS. However, as the clusters get old, the age from red giants is systematically older by a quantity that varies from 0.6 to 0.1 in $\log t$ with respect to the age from the TAMS. This means that either the magnitude difference between the TAMS and CHeB stars has been overestimated by the theoretical isochrones, or, alternatively, that this difference has been underestimated in the observed data. There are several possible ways in which this may occur. Among others we recall: 1) The presence of binary stars that brighten the true position of the

TAMS by as much as 0.6 mag (Maeder 1974). The inclusion of binary stars would reduce the age-discrepancy by as much as 0.2 in $\log t$. 2) The conversion from the theoretical $M_{\rm bol}$ to the observed magnitude M_V, which could be affected by some subtle temperature-dependent error difficult to assess.

As far as the ages determined from the brightest red stars under the assumption that they are at the AGB-tip, these are loosely correlated with the previous two age estimates. Given the strong metallicity dependence of the relation $M_{V\,\rm AGB}(\log t)$, we think that much of the difference can be attributed to uncertainties in the adopted [Fe/H] values for each cluster. Moreover, there is no guarantee that the observed brightest red giants actually correspond to the AGB-tip because 1) the AGB-tip is not well-populated even in the richest clusters, 2) the RGB stars occupy a nearby region of the CMDs, and 3) precise corrections by field contamination are not always possible.

Considering the uncertainties in the ages obtained from the AGB stars, compared to those derived from the TAMS and CHeB stars, we prefer to adopt for the age the simple mean of the logarithmic values between these latter two determinations. The adopted values of the age $\overline{\log t}$ are presented in Table 2.

The age range is reasonably well covered up to ages $\log t = 9.2$. We have already reported that no clusters with ages between 3 and 10 Gyr have been observed in the LMC (Sect. 5.2).

This sample of clusters with known ages can be completed with the six classical globular clusters of the LMC, namely NGC 1466, NGC 1786, NGC 1841, NGC 2210, NGC 2257 and H 11 (see e.g. van den Bergh 1991). As the age determination of these clusters is a topic complicated in itself, no attempt is made to date them; a typical age of 15 Gyr is assumed when necessary.

7. Ages from integrated colors

Elson & Fall (1985a), in a well known study, devised an empirical method for attributing ages to individual clusters from their integrated UBV colors. As already shown in the previous sections, real clusters are affected by a series of effects scattering their integrated UBV colors. Consequently, age does not simply determine cluster colors, and the EF85 method is, by its own nature, subject to a great deal of uncertainty.

In this section we propose two modifications aimed at improving EF85's method and extending its applicability to data sets that go significantly deeper in magnitude.

7.1. Revising the Elson & Fall method

As already commented in Sect. 2.1, the color evolution of SSPs in the $(U-B)$ vs. $(B-V)$ diagram proceeds at an almost constant rate of change of colors by $\Delta\log t$ interval. This is specially true for near-solar metallicity SSPs, in which the only (and not important) deviation from this general rule occurs during the short-lived RSG phase at 10^7 yr. Therefore, the success of the empirical procedure of EF85 is not a surprise. If we divide the $(U-B)$ vs. $(B-V)$ diagram in equally spaced intervals (the parameter S) along the locus of the most rich LMC clusters, there will be a simple linear relationship between the parameter S and the logarithm of cluster ages.

However, there is a main drawback in the EF85 method, when we consider that clusters of different age may have different metallicity mirroring the underlying chemical history of the LMC. For the very old clusters *the linear relation between the parameter S and $\log t$ no longer exists*. This is clearly shown by the color evolution of Models A and B displayed in Figs. 1 and 3: the sequence of old clusters spans a quite large range in colors, but a very small range in $\log t$. Indeed, considering the intrinsic dispersion in colors, we could even say that all clusters along this sequence are coeval. Therefore, drawing the sequence of the S-parameter through the locus of old clusters, would reflect more a sequence of decreasing metallicity at constant age than a sequence of increasing age at constant metallicity. Consequently, the S-method cannot be reliably used in this range of ages in which the metallicity greatly varies.

It should also be noted that the S-sequence defined by EF85 cannot reveal the age gap between 3 and 12 Gyr, simply because their sequence is drawn *along* the line defined by the most populous LMC clusters. In fact, it was shown in Sect. 5.2 that the age gap is not expected to be visible in the $(U-B)$ vs. $(B-V)$ diagram. This explains why Elson & Fall (1988) concluded that no gaps or bursts in the cluster formation history of the LMC are evident in the van den Bergh (1981) sample.

7.2. The definition of the parameter S

In view of the previous discussion, we prefer to redefine the S-sequence basing on our results for the color evolution of SSPs. Differently from EF85, we decided *not to apply the S method to date the old clusters, namely those with E-SWB type VII*. In this group, all the clusters with observed CMD can be classified as classical globulars (see van den Bergh 1991). To these clusters, we attribute a common age of $\log t = 10.2$ (15 Gyr). Although it is not clear whether all the clusters of type VII are indeed so old, their low metallicities (Olszewski et al. 1991; Suntzeff 1992) support this idea.

To derive the S-sequence we proceed as follows. First we compare the empirical S-curve of EF85 (dashed line in Fig. 10) with the locus of the SSP with $Z = 0.008$ (see Fig. 4). A close comparison of the two sequences reveals that they coincide (apart from the short-lived RSG phase) for $B-V < 0.5$. For $B-V > 0.5$ there is a significant difference between the color evolution of the SSP with $Z = 0.008$ and the EF85 S-sequence. This can be understood by considering that their S-sequence was drawn along the lowest boundary of the E-SWB type V clusters, where some populous clusters like NGC 2190, NGC 2162 and NGC 1806 are located. On the contrary, the SSP with $Z = 0.008$ passes through the mean region of E-SWB type V, where other populous clusters like NGC 1783, NGC 1644 and NGC 2154 are observed (see Fig. 5). As discussed in Sect. 5.4, the clusters of E-SWB type V (and VI) are expected to scatter from this line along the direction $\Delta(U-B)/\Delta(B-V) \sim 1.0$. Accordingly, we prefer to interpret the distribution of clusters of E-SWB types V and VI as scatter from the $Z = 0.008$ sequence, and lean on

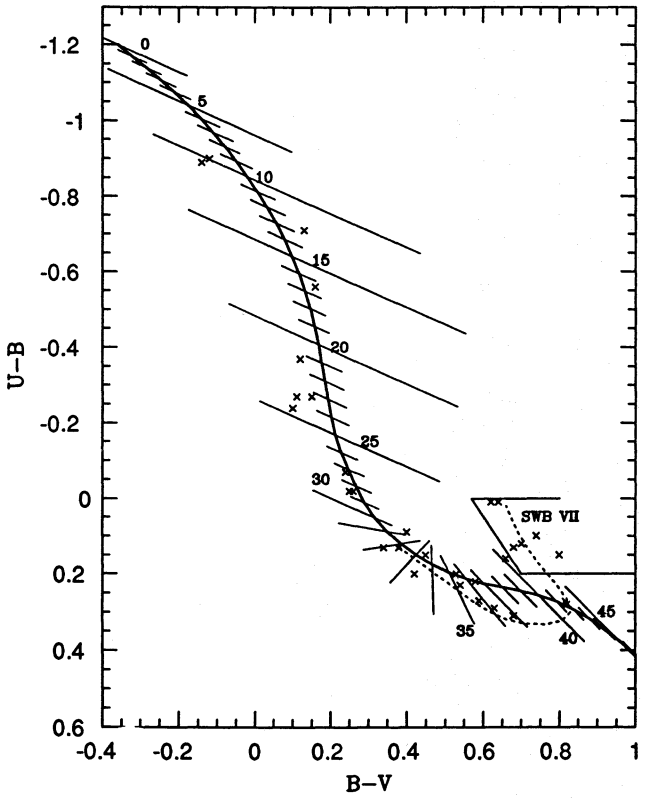

Fig. 10. The adopted sequence of the S-parameter. Superimposed are the clusters used in the age calibration (crosses; see Table 3). Clusters in the area labelled SWB VII are the very old globulars ($\sim$ 15 Gyr). They are not ranked in the S-sequence. The dotted line shows the S-sequence of EF85

this up to $B-V=0.8$. Beyond this color, the $Z=0.008$ sequence continues toward increasing $U-B$. However, the precise form of the S-curve is less of a problem there, because very few clusters with such red colors are observed.

Finally, the S-curve we have adopted is the one of EF85 up to $B-V=0.5$ and of the $Z=0.008$ SSP for redder colors up to $B-V=0.8$. The composite line is shown in Figure 10 together with the equally spaced intervals of $\Delta S=1$ along it.

To assign the S-parameter, EF85 projected each cluster perpendicularly onto the S-curve. Our analysis of the color dispersion by various causes shows that this procedure may not be correct. Therefore, we prefer to project the clusters on the S-curve moving them along the mean dispersion vectors, whose slope varies with the position in the $(U-B)$ vs. $(B-V)$ plane. The slope of the mean dispersion vectors is about $\Delta(U-B)/\Delta(B-V)=0.45$ for the blue clusters, and 1.0 for the red ones (see Fig. 6). Therefore, we divide the region of the $(U-B)$ vs. $(B-V)$ plane occupied by the clusters in strips of constant S, whose slope continuously varies from 0.45 (blue side of the plane) to 1.0 (red side of the plane) as shown in Fig. 10. The portion of the S-curve in the interval $30<S<36$ deserves special care, because it is the region where the mean dispersion vector runs almost parallel to the S-sequence so that assigning the S parameter is intrinsically more uncertain than

Table 3. Photometric data and parameter S for the clusters of Table 1 and the six LMC classical globulars

Cluster	V	$U-B$	$B-V$	S	S_{EF}
NGC 1850A	11.23	−0.89	−0.14	10	–
NGC 1858	9.88	−0.90	−0.12	9	5
NGC 2004	9.60	−0.71	0.13	12	15
NGC 2100	9.60	−0.56	0.16	16	17
NGC 1711	10.11	−0.37	0.12	21	20
NGC 2164	10.34	−0.24	0.10	24	23
NGC 2214	10.93	−0.27	0.11	23	22
NGC 1850	9.57	−0.27	0.15	23	21
NGC 1866	9.73	−0.02	0.25	29	27
NGC 2010	11.72	−0.07	0.24	27	–
NGC 2134	11.05	−0.02	0.26	28	28
NGC 1756	12.24	0.09	0.40	30	32
NGC 2107	11.51	0.13	0.38	32	32
NGC 1831	11.18	0.13	0.34	32	31
NGC 2249	11.94	0.20	0.42	33	34
NGC 1987	12.08	0.23	0.54	35	35
NGC 2108	12.32	0.22	0.58	36	36
NGC 1868	11.57	0.15	0.45	33	33
NGC 2190	12.94	0.29	0.63	36	–
NGC 2209	13.15	0.20	0.53	35	35
NGC 2162	12.70	0.31	0.68	36	39
NGC 2173	11.88	0.28	0.82	41	42
LW 79	13.99	0.27	0.59	35	–
H 4	13.33	0.16	0.66	40	–
NGC 1466	11.59	0.13	0.68	–	48
NGC 1786	10.88	0.10	0.74	–	48
NGC 1841	11.43	0.15	0.80	–	42
NGC 2210	10.94	0.12	0.70	–	48
NGC 2257	12.62	0.01	0.62	–	51
H 11	11.93	0.01	0.64	–	51

in other intervals. Similar remark ought to be made for the very blue and hence young ($\sim 10^7$ yr) clusters, for which the stochastic dispersion is very large.

Neglecting the effect of this color dispersion along directions not perpendicular to the S-sequence, we would probably overestimate the age of the clusters scattered to the red and underestimate that of the clusters scattered to the blue. When applied to the van den Bergh (1981) data, the revised S-method may give ages similar to those from the old one. This because the van den Bergh (1981) sample has little dispersion in the colors. In contrast, it leads to sizable differences when applied to the BCDSP data.

7.3. The Age – S calibration

The clusters with ages determined from the CMD (Table 2) are ranked according to the S-sequence. The values of the S-parameter assigned to them are listed in Table 3, together with the previous determinations by EF85, and the photometric data (integrated magnitudes and colors) by BCDSP.

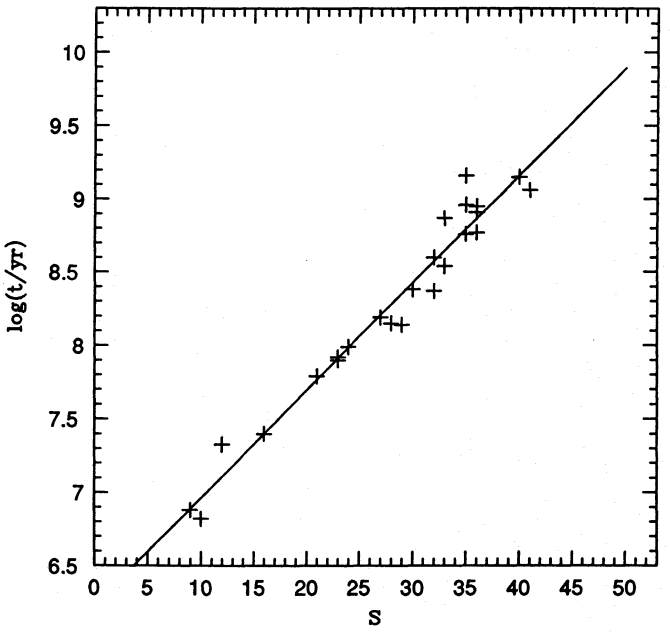

Fig. 11. The S vs. $\log t$ relation for all the clusters with ages derived from the CMD (Sect. 6). The straight line is the unweighted least-squares fit to the data

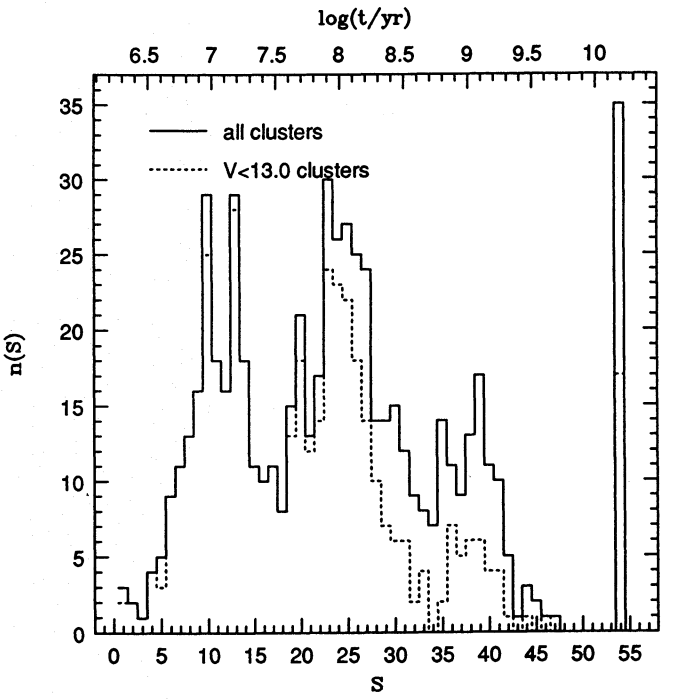

Fig. 12. Histogram of number of clusters vs. S and $\log t$ for the whole BCDSP data sample (solid line). The dashed line shows the same but limited to clusters with $V < 13.0$, which represents the completeness limit

Figure 11 presents a plot of the age ($\log t$) against the S parameter. A linear least-squares fit to the data yields the relation:

$$\log t = (6.227 \pm 0.096) + (0.0733 \pm 0.0032)\ S \qquad (5)$$

with a rms dispersion of 0.137 (in $\log t$) along the line. This relationship has a slope comprised between those of CBB88 and EF85. The rms dispersion is half of that found by EF85, probably because our ages are determined from better data and following a homogeneous procedure.

7.4. The age histogram

With the aid of relation (5) we attribute the ages to all the clusters in the BCDSP catalog. Figure 12 presents the histogram of number of clusters vs. S and $\log t$. The clusters of E-SWB type VII are added to the histogram for the constant age of $\log t = 10.2$, or equivalently $S = 54.2$.

The age histogram of Fig. 12 clearly shows a gap in the number of clusters in the range $44 < S < 54$ or equivalently $9.4 \lesssim \log t < 10.1$, and two major peaks approximately centered at at $S \simeq 23$ and $S \simeq 39$, to which ages of 10^8 and 10^9 yr correspond, respectively. We provisionally interpret these peaks as periods of enhanced cluster formation. There is another peak at about $S = 10$, age of a few 10^7 yr, which cannot be safely interpreted in a similar way, because at these ages the sample contains many objects that probably are not clusters (see Sect. 5).

This age histogram remarkably resembles the one presented by van den Bergh (1991) that was derived from the age compilation of Sagar & Pandey (1989).

8. The corrected ADF

8.1. The fading lines

The distribution of cluster ages shown in Fig. 12 reflects not only the global history of cluster formation and destruction in the LMC, but also the fading of the cluster luminosities with the age caused by the evolution of the component stars. In order to single out and correct for this effect, we need to compute the ADF for a sample of clusters with the same initial luminosities.

Figure 13 presents the distribution of ages and magnitudes for the BCDSP data, known to be reasonably complete down to $V = 13.0$. Superimposed are the fading lines $M_V(t)$ obtained from the $Z = 0.008$ SSP (see Sect. 2). They delimit the regions in which clusters have the same initial masses and hence the same initial luminosities (assuming that the decrease in the luminosity is due only to the natural evolution of the component stars). Two choices for the slope of the IMF, i.e. $x = 1.35$ and 2.5, are considered in order to investigate the effect of different IMFs on the final ADF.

With $x = 2.5$ it is possible to sample a group of clusters which remain brighter than $V = 13.0$ all over the entire age range. This is no longer possible with $x = 1.35$, because any significant sample of clusters becomes incomplete at ages $\log t \gtrsim 8.5$. In such a case, an estimate of the incompleteness in the data is required also for clusters fainter than $V = 13.0$.

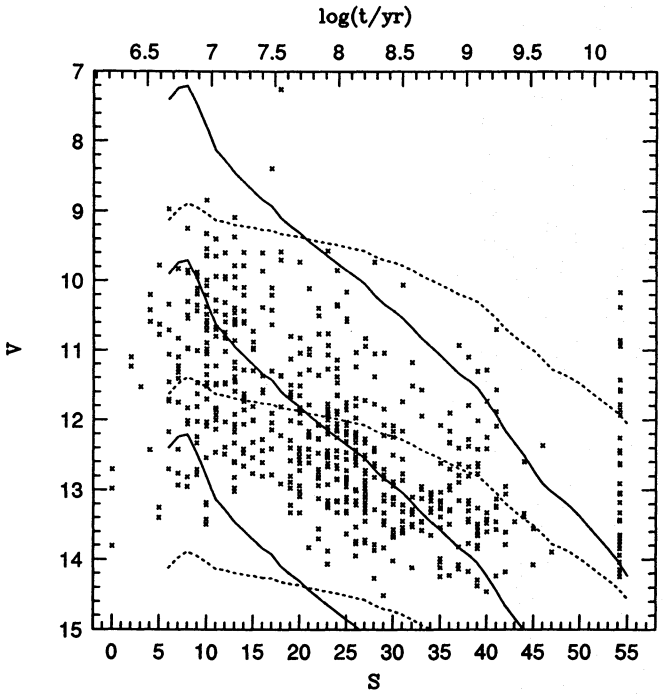

Fig. 13. Distribution of ages and magnitudes for the BCDSP sample (crosses). Superimposed are the fading lines for an SSP with $Z = 0.008$ and different initial total mass (10^3, 10^4 and 10^5 $M_\odot$ from bottom to top, according to the normalization adopted by GB93) with a distance modulus $(m - M)_0 = 18.5$ to the LMC. Solid lines are for an IMF with $x = 1.35$, whereas the dotted lines are the same but with $x = 2.5$

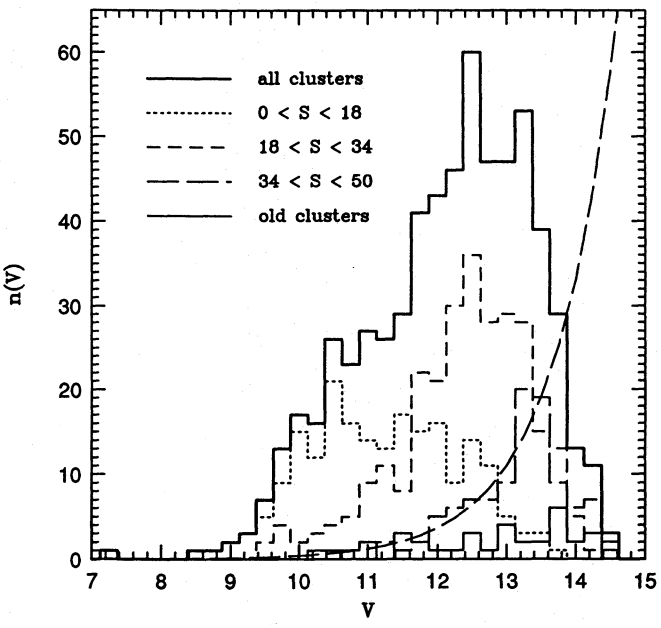

Fig. 14. Luminosity functions for LMC clusters in different S (age) intervals. For the clusters in the range $34 < S < 50$, we plot also the power law $\log n(V) = -5.2 + 0.48\,V$ fitted to the number of clusters in the interval $11.0 < V < 13.25$. This power law is used to estimate the incompleteness factors up to $V = 14.0$

8.2. Correction for incompleteness

Figure 14 shows the histogram of number of clusters vs. the V magnitude for several intervals of parameter S and hence age. The LF is clearly different for the different samples. The one for the older clusters, in particular, closely follows a power law with the number of clusters increasing with magnitude up to $V \simeq 13$. Beyond this, the LF drops, indicating that the incompleteness limit of the sample has been reached.

In the case of the IMF with slope $x = 1.35$, the correction for incompleteness is required already for clusters in the range $34 < S < 50$. To this purpose, we fit with a power law the luminosity function for the clusters in the interval $11.0 < V < 13.25$, and get the reference LF from which we derive the incompleteness correction in the intervals of fainter magnitudes. The analytical LF is expressed by $\log n(V) = -5.2 + 0.48\,V$ (dashed line in Fig. 14). It corresponds to a LF of the form $n(L) \propto L^{-\alpha}$ with index $\alpha \simeq 2.2$. Our index α is greater than the $\alpha = 1.5$ derived by Elson & Fall (1985b) from complete samples of clusters in two areas of the LMC. As pointed out by the latter authors, $\alpha > 2$ implies that the total luminosity of the cluster sample diverges, which of course is not real. Despite this difficulty, we assume our power law to be representative of the true LF down to $V = 14.0$ for the clusters in the interval $34 < S < 50$. Defining the incompleteness factors as the ratio between expected and observed number of clusters, we get 1.1 at $V = 13.5$, 2.8 at $V = 13.75$, and 8.3 at $V = 14.0$. The value for $V = 14.0$ is however highly uncertain due to the small number of clusters observed at this magnitude.

For the old clusters (the E-SWB VII ones), the estimate of incompleteness is problematic. In order to calculate the ADF at these ages for the case $x = 1.35$, we should suppose that the above power law can be extended up to $V \sim 16.0$ mag. Since such an assumption is obviously risky, we prefer not to apply incompleteness corrections to clusters with $V > 14$.

8.3. The corrected ADF

Cluster counts in the mass-limited strips over age bins corresponding to $\Delta S = 2$ are performed and corrected for incompleteness in order to derive the ADF – number of clusters by age interval, $\mathrm{d}N_{\rm cl}/\mathrm{d}t$ – shown in Fig. 15, both for $x = 1.35$ and 2.5.

Two distinct bumps can be noticed in the ADF, one for $\log t \simeq 8.0$, the other for $\log t \simeq 9.1$, similarly to what has already been seen in Fig. 12, and the age gap is seen in the range $9.6 \lesssim \log t < 10.1$. Remarkably, the bump at $\log t \simeq 9.1$ is present even before correcting for incompleteness. The bump at $\log t \simeq 7.0$ is caused by the presence of a significant number of young associations in the BCDSP sample, whose detailed discussion is beyond the scope of this paper. Finally, the ADF obtained for the old clusters likely constitutes a lower limit to the real one, because the incompleteness factors are probably largely underestimated for these clusters.

The ADFs shown in Fig. 15 now represent the result of the history of cluster formation and destruction in the LMC. The

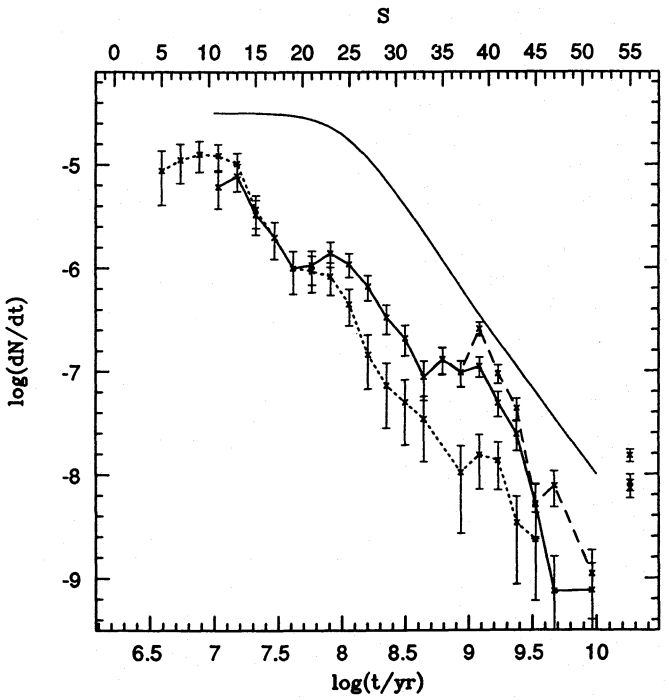

Fig. 15. ADFs calculated for the case $x = 1.35$ (thick solid line) and the case $x = 2.5$ (dotted line). For the case $x = 1.35$ we plot also the ADF corrected for incompleteness (thick dashed line). The error bars indicate the statistical uncertainty of the counts ($\sqrt{\mathrm{d}N_{\mathrm{cl}}}/\mathrm{d}t$). The thin solid line is the Wielen (1971) ADF for the solar neighbourhood, vertically shifted by an arbitrary constant

destruction processes alone, acting on a sample of clusters with constant formation rate, are expected to generate smooth ADFs, just like that derived by Wielen (1971) for the sample of Galactic clusters in the solar neighbourhood. Since the dynamical processes of dissolution-disruption of clusters (see Wielen 1991) are likely the same in the Galactic Disk and in the LMC (although differing in their intensities and time-scales), the bumps and gaps in the ADF of the LMC clusters can only be interpreted as genuine episodes of enhanced and reduced cluster formation.

Noteworthy, no arbitrary shift has been applied to the ADFs of the LMC clusters shown in Fig. 15. For young clusters up to ages 10^8 yr, which are probably not yet affected by the dynamical effects of dissolution-disruption, the value of $\mathrm{d}N_{\mathrm{cl}}/\mathrm{d}t$ represents a lower limit to the present global cluster formation rate of the LMC. At 10^8 yr we have $\mathrm{d}N_{\mathrm{cl}}/\mathrm{d}t \simeq 10^{-6}$ clusters yr^{-1} for both choices of x. Values at least 4 times larger would be obtained with the inclusion of all the clusters with $V < 13$ at this approximate age. These values agree with the cluster formation rate of 2.7×10^{-6} yr^{-1} estimated by Hodge (1988) from studies of complete samples of clusters in 12 fields of the LMC.

Concerning the mean slope of the ADF, it has been suggested that slopes flatter than in the Galactic case should probably indicate a slower destruction rate resulting from the lower tidal field of the LMC. We believe that this conclusion is premature for two reasons. Firstly, the slope of the ADF is very sensitive to the slope of the IMF. Indeed if $x \gtrsim 2.5$ we can obtain ADFs that are even steeper than the Galactic ADF (Wielen 1971). This is a point of high uncertainty because the slope of the IMF is not firmly established and there are also observational hints suggesting that the slope can vary from cluster to cluster (Mateo 1990). Secondly, the ADF probably suffers from the discontinuous history of cluster formation in the LMC, and therefore arguing about dynamical effects on the base of a *mean* slope may be hazardous.

The epochs of the bumps noticed in the ADF are in good agreement with the episodes of enhanced cluster and star formation found by different authors using different data. Specifically, studying the CMD of 31 clusters in external regions of the LMC, Mateo (1988b) suggested that a burst of cluster formation occurred in the age interval 2 to 4 Gyr. Frogel et al. (1990) reported two peaks in the color distribution of M stars in LMC clusters, corresponding to ages $\sim$ 100 Myr and $\gtrsim$ 1 Gyr; both peaks were also present in a sample of M stars in the LMC bar (Frogel & Blanco 1983). Wood et al. (1985) found similar evidence of epochs of enhanced star formation in the distribution of periods and luminosities of field long-period variables and Cepheids. Analysing the CMD of field stars in selected regions of the LMC, Bertelli et al. (1992) concluded that a major episode of star formation started $\sim$ 4 Gyr ago.

Our results differ from the previous ones by EF85, Elson & Fall (1988), and CBB88, who basing on UBV data did not find convincing evidence for epochs of enhanced or reduced cluster formation rate[2]. Part of the difference can be attributed to the better statistics provided by BCDSP sample with respect to the old one by van den Bergh (1981) and part to having considered the mean slope of the dispersion vector in the derivation of the parameter S. However, the major reason resides in the different method we have adopted to attribute ages to the red clusters.

8.4. The effect of the ADF on the color gaps

In Sects. 5.3 and 5.4 we concluded that the gross characteristics of both the gaps in the distribution of $B - V$ colors and the gap in the $(U - B)$ vs. $(B - V)$ diagram can be naturally explained by a continuous distribution of clusters along the evolutionary sequences determined by the general law of metal enrichment of the LMC. However, some marginal disagreement between theoretical predictions and observational data suggests that we were not using the right ADF. In the following we check whether the ADF we have derived can improve upon those points of disagreement.

With respect to the bimodal distribution of $B - V$ colors, we note that the two peaks noticed in the ADF at ages of 10^7 and 10^8 yr occur when the integrated colors are $(B - V)_0 \simeq 0.2$ and 0.7, respectively. It coincides with the position at which the peaks in the $B - V$ histogram occur, suggesting that the particular form of the ADF contributes to enhance the bimodal distribution of the $B - V$ colors. In order to test it and to keep the

[2] An exception worth of notice is the ADF obtained by Alongi & Chiosi (1991), which shows both the 100 Myr and 2 Gyr bumps.

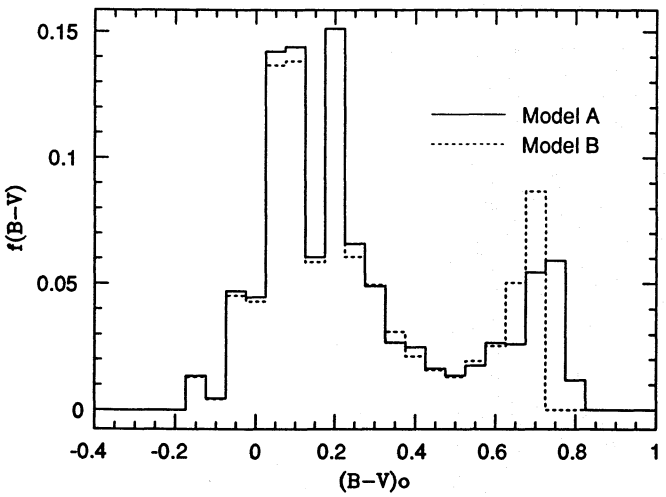

Fig. 16. Simulated histogram of $B-V$ colors, assuming an age distribution $f(t)$ which includes the gaps and bumps of the observed one (Fig. 12)

analysis simple, we make a simulation of the $B-V$ histogram in which we suitably modify the analytical ADF $f(t) \propto t^{-1}$ by adding the peaks and gaps suggested in the age histogram of Fig. 12.

The results of the simulation are shown in Fig. 16. Compared to the case with $f(t) \propto t^{-1}$ of Fig. 9b, the following differences are evident: 1) The peak at the reddest colors $[(B-V)_0 \simeq 0.8]$ is decreased by the introduction of the gap in the age range $9.3 < \log t < 10.1$. 2) The bumps at $8.0 < \log t < 8.5$ and $9.0 < \log t < 9.3$ somewhat enhance the peaks at the positions $(B-V)_0 = 0.2$ and $(B-V)_0 = 0.7$, respectively. Assuming a mean reddening of $E(B-V) = 0.07$, the colors of the peaks exactly agree with the observed ones.

The presence of a pronounced peak at $(B-V)_0 = 0.1$ in the simulations requires some explanation. This peak is generated by the near-zero $\mathrm{d}(B-V)/\mathrm{d}t$ derivative [see eq. (4)] at ages of about $\log t \simeq 7.1$. However, as at these ages stochastic effects are expected to be very severe and to scatter the colors of the clusters, the peak itself should spread over a much larger range of colors and hence decrease if not disappear.

With respect to the gap in the $(U-B)$ vs. $(B-V)$ diagram (Sect. 5.4), we notice that it occurs at $S \simeq 34$, corresponding to an age of $\sim$ 500 Myr. It strongly suggests that in the gap region the scarcity of clusters along the mean evolutionary sequence owns its origin to the period of reduced cluster formation between the 100 Myr and 1–2 Gyr bursts suggested by the analysis of the ADF. This corresponds to the lower end of the box showing in Fig. 5 the BCDSP gap. The absence of clusters in the upper end of the box is determined by the natural dispersion of the colors, as concluded in Sect. 5.4. This interpretation of the BCDSP gap is confirmed by theoretical simulations of the $(U-B)$ vs. $(B-V)$ plane calculated assuming the same total number of clusters as in the observational sample, a reasonable AMR, all possible causes of color dispersion (Sect. 5.1), and the age distribution function $f(t)$ inferred from the observation.

9. Concluding remarks

The main results of this work are schematically presented in the abstract.

We present just a final consideration: This paper clarifies that a set of evolutionary models of SSPs that smoothly evolve in the $(U-B)$ vs. $(B-V)$ diagram (in agreement with the linear relationship S vs. $\log t$ found in the data) can lead to a good description of the features observed in the distribution of UBV colors of LMC clusters, provided that we consider: 1) a reasonable AMR, 2) the natural dispersion induced in the observed colors by different causes. The detailed distribution of the colors, however, can only be explained by the presence of gaps and peaks in the history of cluster formation, which in turn have been already indicated by a series of independent observational data. There is no need of invoking rapid changes in the integrated colors of SSPs in order to explain the apparent gaps in the colors.

Acknowledgements. We are greatly indebted to E. Bica for making available its data prior to publication, and for the many remarks which helped to improve the final version of this paper. L. Girardi acknowledges a fellowship from the Brazilian funding agency CNPq and the hospitality from the Department of Astronomy of the Padova University. This study has been financed by the Italian Ministry of University, Scientific Research and Technology (MURST) and the Italian Space Agency (ASI).

References

Alongi M., Chiosi C., 1989, in: Astrophysical Ages and Dating Methods, eds. E. Vangioni-Flam et al., Editions Frontières: Gif sur Yvette, p. 207
Alongi M., Chiosi C., 1991, in: The Magellanic Clouds, IAU Symp. 148, eds. R. Haynes and D. Milne, Dordrecht: Reidel, p. 193
Battinelli P., Capuzzo-Dolcetta R., 1989, ApJ 347, 794
Bertelli G., Bressan A., Chiosi C., Fagotto F., Nasi E., 1994, A&AS 106, 275
Bertelli G., Bressan A., Chiosi C., Mateo M., Wood P.R., 1993, ApJ, 412, 160
Bertelli G., Mateo M., Chiosi C., Bressan A., 1992, ApJ 388, 400
Bica E., Alloin D., 1986, A&A 162, 21
Bica E., Clariá J.J., Dottori H., Santos Jr. J.F.C., Piatti A., 1991, ApJ 381, L51
Bica E., Clariá J.J., Dottori H., Santos Jr. J.F.C., Piatti A., 1992a, in: The Stellar Populations of Galaxies, IAU Symp. 149, eds. B. Barbuy and A. Renzini, Dordrecht: Kluwer, p. 392
Bica E., Clariá J.J., Dottori H., 1992b, AJ 103, 1859
Bica E., Clariá J.J., Dottori H., Santos Jr. J.F.C., Piatti A., 1994, in preparation. (BCDSP)
Bressan A., Chiosi C., Fagotto F. 1994, ApJS 94, 63
Bressan A., Fagotto F., Bertelli G., Chiosi C., 1993, A&AS 100, 647
Buonanno R., Corsi C.E., Fusi-Pecci F., Greggio L., Renzini A., Sweigart A.V., 1988, in: Globular Clusters Systems in Galaxies, IAU Symp. 126, eds. J.E. Grindlay and A.G. Davis Philip, Dordrecht: Reidel, p. 555
Burstein, D., Heiles, C. 1984, ApJS, 54, 33
Cassatella A., Barbero J., Geyer E.H., 1987, ApJS 64, 83
Chiosi C., Bertelli G., Bressan A., 1988, A&A 196, 84 (CBB88)

Chiosi C., Bertelli G., Bressan A., 1992, ARA&A 30, 305
Chiosi C., Bertelli G., Meylan G., Ortolani S., 1989, A&A 219, 167
Cohen J.G., 1982, ApJ 258, 143
Corsi C.E., Buonanno R., Fusi-Pecci F., Ferraro F.R., Testa V., Renzini A., Greggio L., 1994, MNRAS, in press
Cowley A.P., Hartwick F.D.A., 1982, ApJ 259, 89
Da Costa G.S., 1991, in: The Magellanic Clouds, IAU Symp. 148, eds. R. Haynes and D. Milne, Dordrecht: Reidel, p. 183
Djorgovski S.G., Meylan G., 1993, ESO Scientific Preprint no. 932
Elson R.A.W., 1986, PhD Thesis, University of Cambridge
Elson R.A.W., Fall S.M., 1985a, ApJ 299, 211 (EF85)
Elson R.A.W., Fall S.M., 1985b, PASP 97, 692
Elson R.A.W., Fall S.M., 1988, AJ 96, 1383
Fagotto F., Bressan A., Bertelli G., Chiosi C., 1994a, A&AS 104, 365
Fagotto F., Bressan A., Bertelli G., Chiosi C., 1994b, A&AS 105, 29
Ferraro F.R., Fusi-Pecci F., Testa V., Greggio L., Corsi C.E., Buonanno R., Terndrup D.M., Zinnecker H., 1994, MNRAS, in press
Frenk C.S., Fall S.M., 1982, MNRAS 199, 565
Frogel J.A., Blanco V.M., 1983, ApJ 274, L57
Frogel J.A., Mould J., Blanco V.M., 1990, ApJ 352, 96
Girardi L., Bica E., 1993, A&A 274, 279 (GB93)
Hodge P., 1988, PASP 100, 576
Kurucz R.L., 1992, in: The Stellar Populations of Galaxies, IAU Symp. 149, eds. B. Barbuy and A. Renzini, Dordrecht: Kluwer, p. 225
Maeder A., 1974, A&A 32, 177
Maeder A., Meynet G., 1989, A&A 210, 155
Mateo M., 1988a, ApJ 331, 261
Mateo M., 1988b, in: Globular Clusters Systems in Galaxies, IAU Symp. 126, eds. J.E. Grindlay and A.G. Davis Philip, Dordrecht: Reidel, p. 557
Mateo M., 1990, in Physical Processes in Fragmentation and Star Formation, eds. R. Capuzzo-Dolcetta, C. Chiosi, & A. Di Fazio, Dordrecht: Kluwer Acad. Publ., p. 401
Mateo M., Hodge P., 1987a, ApJ 320, 626
Mateo M., Hodge P., 1987b, ApJS 60, 893
Olszewski E.W., Schommer R.A., Suntzeff N.B., Harris H.C., 1991, AJ 101, 515
Panagia N., Gilmozzi R., Macchetto F., Adorf H.M., Kirshner R.P., 1991, ApJ 380, L23
Persson S.E., Aaronson M., Cohen J.G., Frogel J.A., Matthews K., 1983, ApJ 266, 105
Racine R., 1973, AJ 78, 180
Renzini A., Buzzoni A., 1986, in: Spectral Evolution of Galaxies, eds. C. Chiosi and A. Renzini, Dordrecht: Reidel, p. 195
Sagar R., Pandey A.K., 1989, A&AS 79, 407
Sagar R., Richtler T., de Boer K.S., 1991a, A&AS 90, 387
Sagar R., Richtler T., de Boer K.S., 1991b, A&A 249, L5
Searle L., Sargent W.L.W., 1972, ApJ 173, 25
Searle L., Wilkinson A., Bagnuolo W.G., 1980, ApJ 239, 803 (SWB)
Seggewiss W., Richtler T., 1989, in Recent Developments in MC Research, eds. K.S. de Boer, F. Spite, G. Stasinska, p. 45
Smith H.A., Searle L., Manduca A., 1988, in: Globular Clusters Systems in Galaxies, IAU Symp. 126, eds. J.E. Grindlay and A.G. Davis Philip, Dordrecht: Reidel, p. 563
Suntzeff N.B., 1992, in: The Stellar Populations of Galaxies, IAU Symp. 149, eds. B. Barbuy and A. Renzini, Dordrecht: Kluwer, p. 23
Vallenari A., Chiosi C., Bertelli G., Meylan G., Ortolani S., 1991, A&AS 87, 517
Vallenari A., Chiosi C., Bertelli G., Meylan G., Ortolani S., 1992, AJ 104, 1100
Vallenari A., Aparicio A., Fagotto F., Chiosi C., 1994a, A&A 284, 424
Vallenari A., Aparicio A., Fagotto F., Chiosi C., Ortolani S., Meylan G., 1994b, A&A 284, 447
van den Bergh S., 1981, A&AS 46, 79
van den Bergh S., 1991, ApJ 369, 1
Wielen R. 1971, A&A 13, 309
Wielen R. 1988, in: Globular Clusters Systems in Galaxies, IAU Symp. 126, eds. J.E. Grindlay and A.G. Davis Philip, Dordrecht: Reidel, p. 393
Wood P.R., Bessell M.S., Paltoglou G., 1985, ApJ 290, 477

This article was processed by the author using Springer-Verlag LaTeX A&A style file version 3.